Chapter 4

The Effects of Cold Work, Recovery and Strain Aging on the Hardness of Aged Cold-worked 430

This chapter is the first of five which report the results of the experimental measurements which were outlined in chapter 3. It is aimed at elucidating the effects of cold work, recovery and strain aging. Cold work increases the strength of the material by work hardening; recovery during aging would tend to decrease this strengthening effect, while strain aging is expected to enhance it.

4.1. Effect of Cold Work on the hardness and aging behaviour of as-received sheet material (8mm thick)

4.1.1. Hardness and Microstructure

It was found that a 38% reduction in area through cold rolling (in the original rolling direction) raised the Vickers hardness of the material by 100 kg/mm^2 from an original hardness of 167 kg/mm^2.

Cold rolling also caused changes in the microstructure; these changes were less apparent under the optical microscope (figure 4.1) than during examination in a transmission electron microscope (figure 4.2). The steel consists at room temperature (and in the equilibrium state) of ferrite and carbides (visible as black dots in figure 4.1).

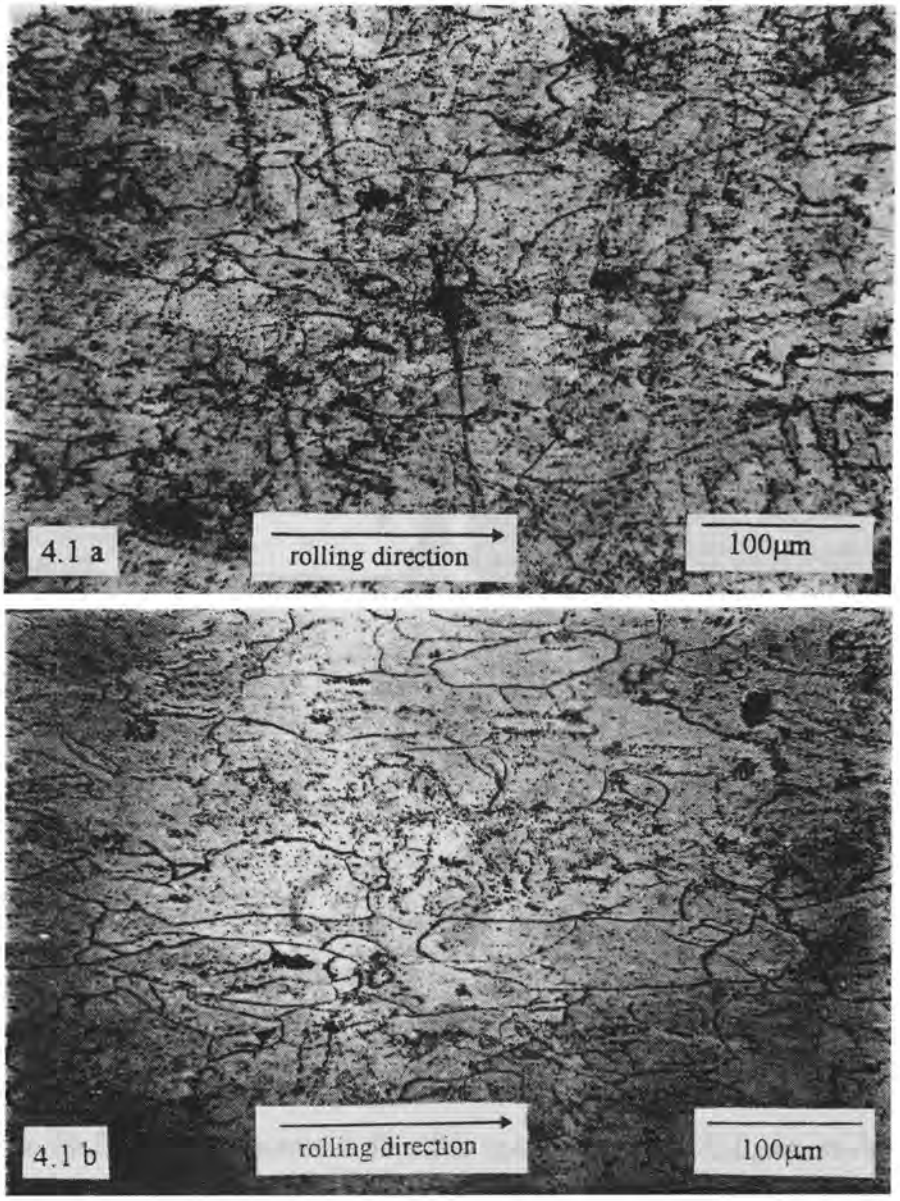

***Figure 4.1**: Microstructure of (a) as-received sheet material - 8mm thick, and (b) sheet material after cold rolling - 38% reduction in area (5mm thick)*

Cold work increases the number of dislocations and distorts the structure, and the pronounced elongated structure in the rolling direction is clearly visible (figure 4.1(b)).

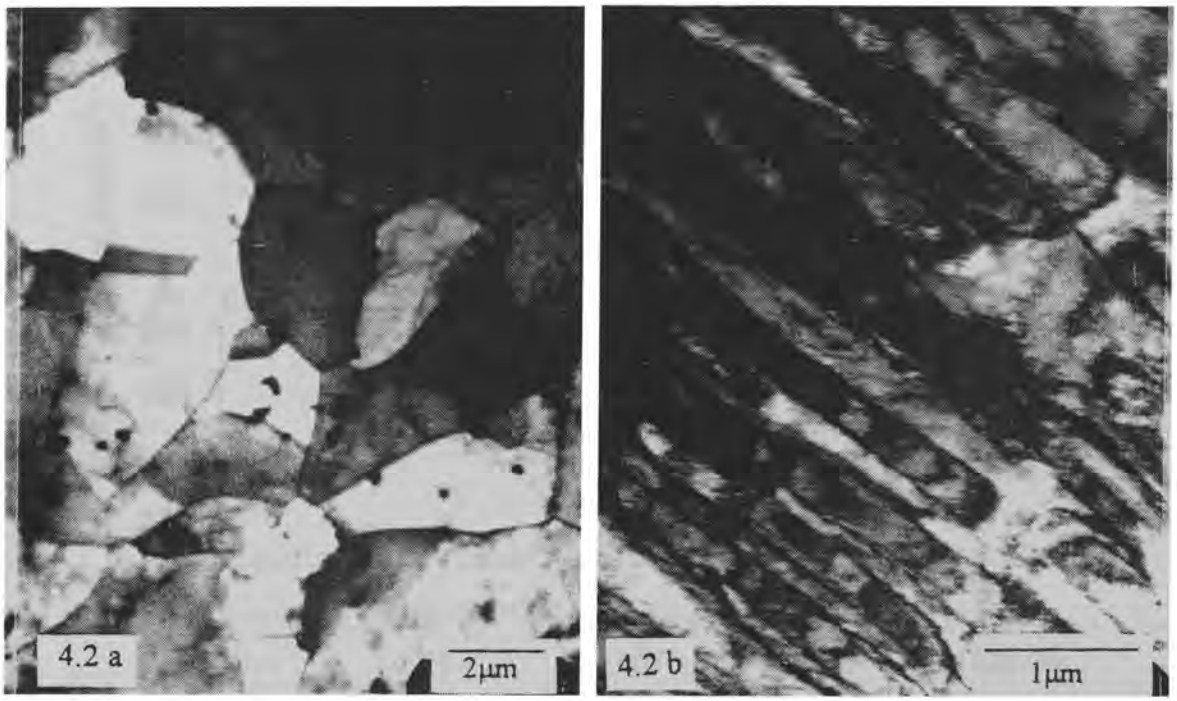

***Figure 4.2**: TEM micrographs (bright field) of as-received material (a) before cold work and (b) after cold work (38% reduction in area), indicating dislocation-rich layers after cold rolling*

In some regions of the as-received material smaller grains could clearly be seen, but overall the material consisted of large grains with a low dislocation density. This type of structure is that expected for an annealed ferritic stainless steel (Krauss 1989). Precipitates were also visible e.g. as black dots in figure 4.2(a). After cold rolling, the dislocation-rich layers running in one direction became very prominent (figure 4.2(b)).

4.1.2. Aging Behaviour

Figure 4.3 shows the hardness after aging at 475°C for different periods, with and without prior cold work. It is revealed by the curves that for the material that was cold worked the initial increase in hardness (at t = 0.5 h) is more pronounced than for the material that did not receive any cold rolling. The aging behaviour at longer periods of aging is similar with and without cold working - a hardness increase occurs for aging beyond 100 hours in both cases. That is to say, the stage where α" is the prime strengthening mechanism (refer to section 6.5.2) does not seem to be affected by deformation.

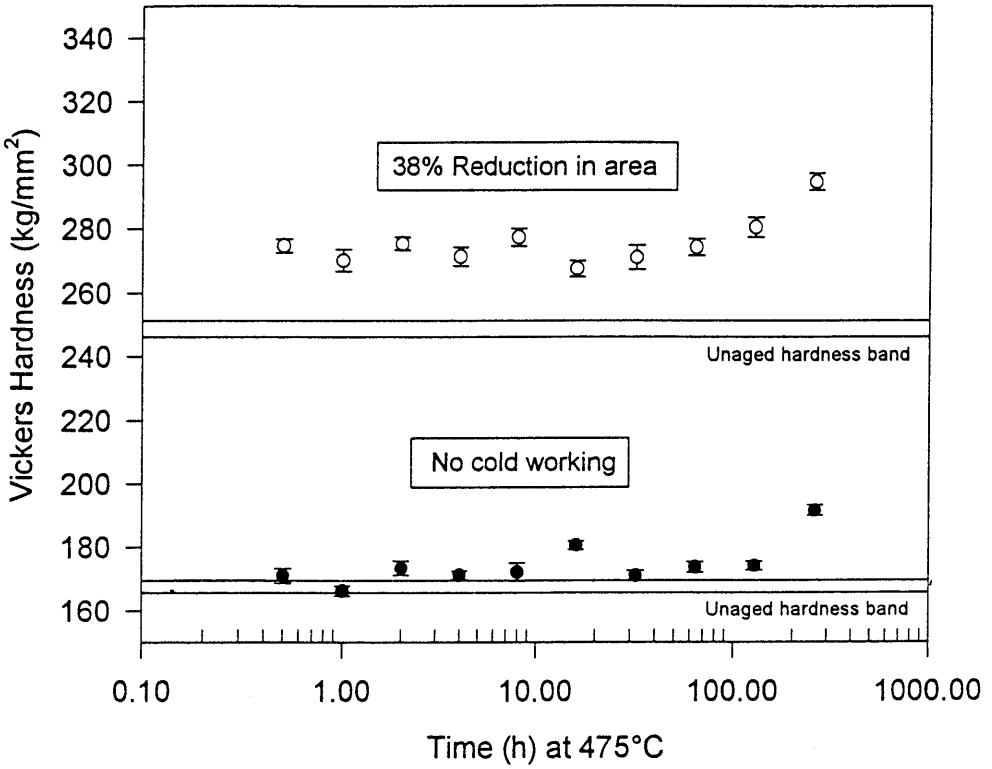

***Figure 4.3**: Comparison of aging behaviour (at 475 ℃) of sheet material, solution treated at 920 ℃ for 15 minutes, before and after cold rolling (38% reductiuon in area). 95% confidence intervals are shown. Hardening behaviour is similar for long periods of aging*

It is known that cold working, because it increases the internal energy or strain of a material, causes an increased nucleation of second phase particles (Tisinai and Samans 1957). This probably accounts for the more pronounced initial increase in hardness (at t = 0.5 h) of the cold worked material, as it is energetically more favourable for the carbides and nitrides to precipitate.

When the general corrosion resistance of the treated material was examined, the samples that were not cold rolled and aged for intermediate periods at 475°C, formed second anodic current peaks (associated with sensitisation (Mao and Zhao 1993)) at 0V. These peaks disappeared again with longer aging. The cold worked material did not exhibit the same behaviour.

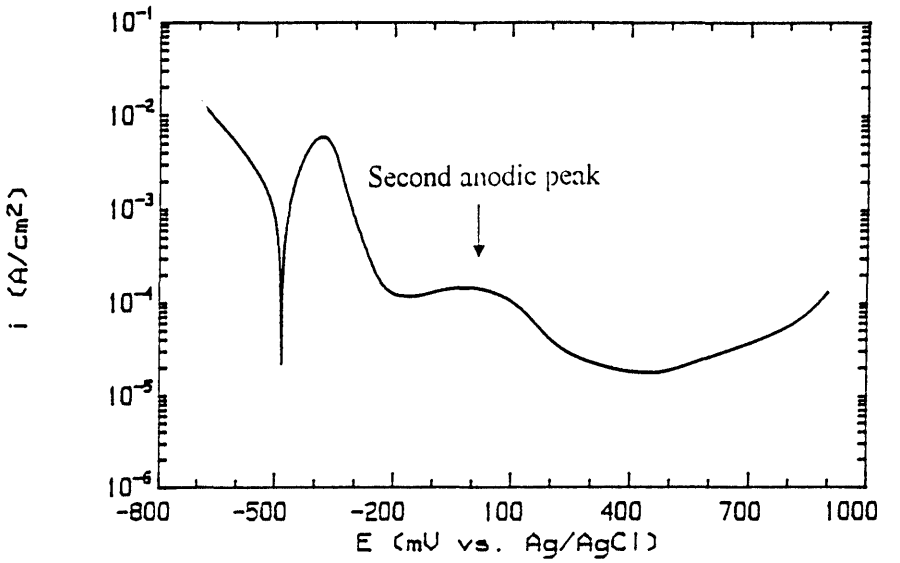

***Figure 4.4**: Polarisation diagram showing second anodic current peak of sheet material solution treated at 920 ℃, water quenched and aged at 475 ℃ for 64 hours (0.5 M H_2SO_4 test solution)*

For the material that was not cold rolled prior to aging, the precipitation of Cr-rich carbides and nitrides (causing localised chromium depletion of the matrix) and reduction of this depletion at the longer aging times (as Cr diffuses to the impoverished areas), are thought to explain the appearance and subsequent disappearance of the anodic peak.

In the cold rolled material, cold working, in addition to increasing the dislocation density and internal (strain) energy, also has an influence on the nucleation of carbides. This might offer the reason for the absence of second anodic current peaks in the heavily deformed material. In an annealed material carbides form essentially on the grain boundaries during aging. In this way a continuous area, depleted in chromium, is formed. This area is very sensitive to corrosion. With increasing amounts of cold work prior to aging, heating at the aging temperature results in progressively more widespread precipitation of carbides within the grains. This presumably shortens the diffusion paths for chromium, and along with the expected faster Cr diffusion rate in cold worked metal, can result in the total absence of sensitisation in highly cold worked material (Pednekar and Smialowska 1980).

4.2. Recovery

4.2.1. Background

A cold worked material, being in a state of higher energy, is thermodynamically unstable. With thermal activation, such as provided by annealing, the material tends to transform to states of lower energies through a sequence of microstructural changes. The first stage is known as recovery. As recovery proceeds, the following emerge: the annealing out of point defects and their clusters, the annihilation and rearrangement of dislocations, polygonisation and the forming of recrystallisation nuclei energetically capable of further growth. These structural changes do not involve high-angle boundary migration (ASM Metals Handbook vol 9, 1985, p. 692,693). The principal effect of recovery seems to be the relief of internal stresses caused by cold working, while the mechanical properties are essentially unchanged (Dieter 1988, p. 233).

4.3.2. Aging at 475°C

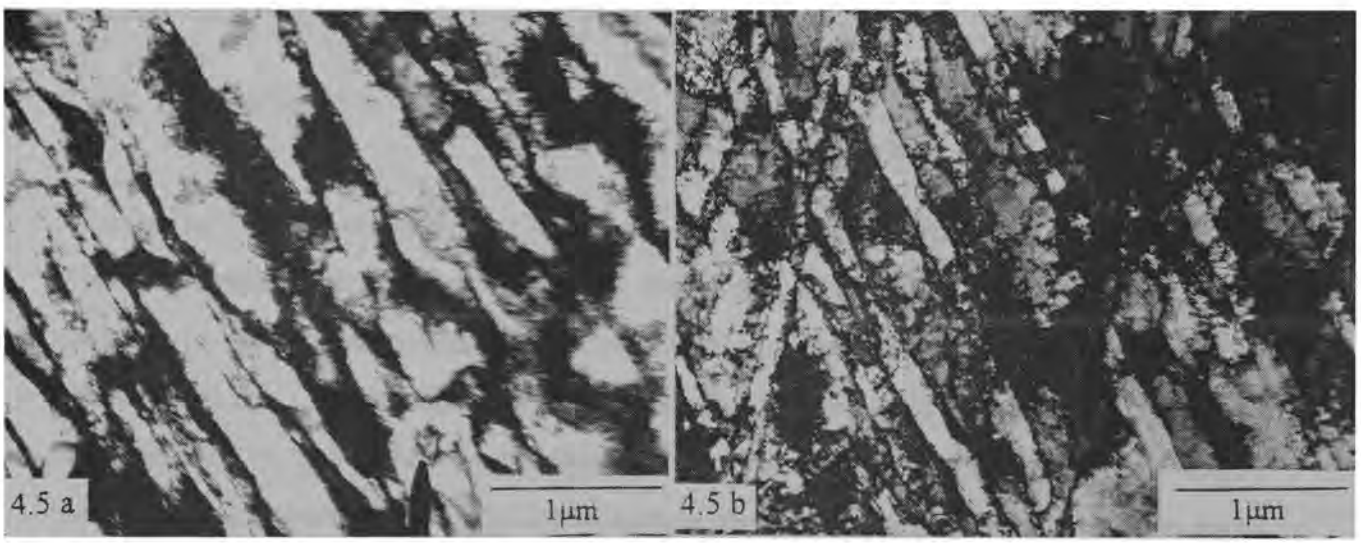

***Figure 4.5**: TEM micrograph (bright field) of the matrix after cold working with (a) no aging and (b) aging at 475 ℃ for 260 hours, indicating that recovery occurs with aging*

The thin ribbon-like structure, characteristic of cold worked material, is clearly visible in the unaged material (figure 4.5(a)). The structure is formed by dislocation-rich layers running in the same direction. As deformation by cold work proceeds, cross slip takes place, and the cold-worked structure forms high dislocation density regions or tangles, which develope into tangled networks. Thus the characteristic structure of the cold worked state is a cellular substructure in which high-density-dislocation tangles form the cell walls (Dieter 1988, p. 230).

With aging, the cell boundaries became more definite in appearence. This parallelogram structure is formed by dislocation double walls running in two directions. The double walls are two thin dislocation walls parallel to a crystallographic slip plane (Dymek and Blicharski 1985). The cells are bound by low angle grain boundaries which form as dislocations group together in low energy arrangements. This results in the formation of a subgrain structure in which the centre of each grain is relatively dislocation-free.

The TEM micrographs indicate that recovery does occur during aging, but no recrystallisation is observed.

4.3. Strain Aging

4.3.1. Background

Strain aging is the phenomenon by which a cold-worked steel hardens by the formation of interstitial solute atom atmospheres around dislocations. The dislocation sources that were active in the deformation process just before cessation of the deformation operation, are thus pinned down as a result of the aging process. Because solute atoms must diffuse through the lattice in order to accumulate around dislocations, strain aging is a function of time; and of temperature, inasmuch as diffusion is temperature dependent (Reed-Hill 1992). Strain aging of steel causes a loss of ductility and a corresponding increase in hardness, yield strength and tensile strength. Strain aging may occur at ambient temperature, but the rate can be considerably enhanced by aging at higher temperatures; for instance, strain aging may occur within a few minutes at 200°C (ASM Metals Handbook vol. 8, 1985, p. 12).

To acertain whether strain aging contributes to the total strengthening effect, aging heat treatments were performed at 100°C on chain links and sheet material.

4.3.2. Aging at 100°C

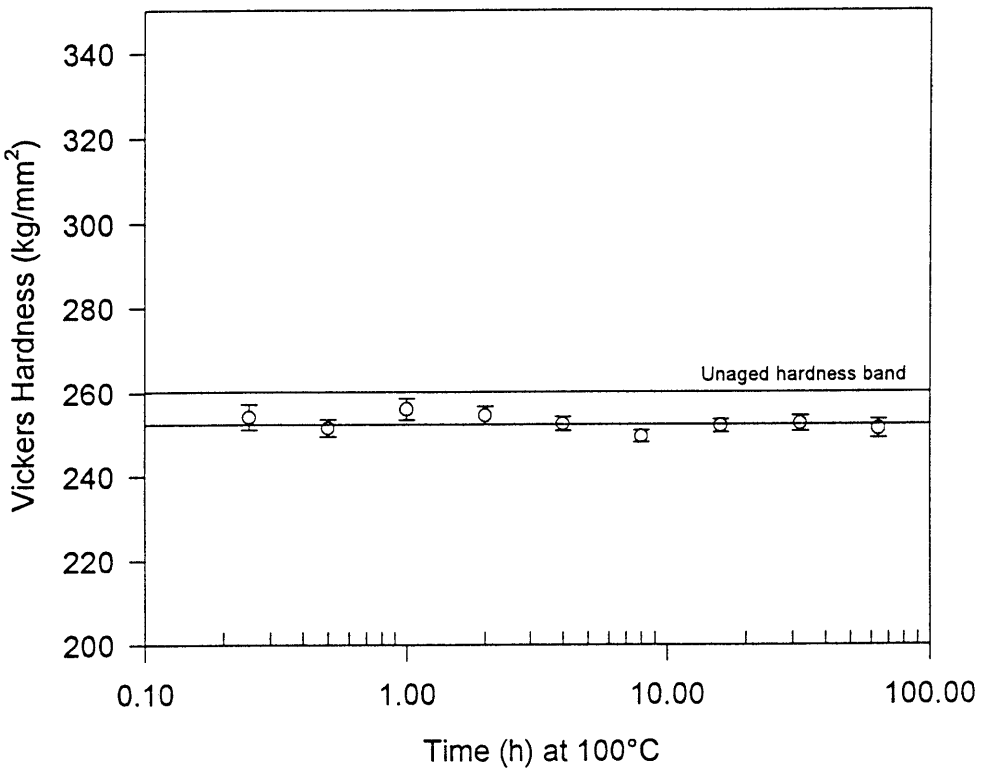

***Figure 4.6**: Hardness of Chain links aged at 100℃, indicating that no strain aging occurs. 95% confidence intervals are shown*

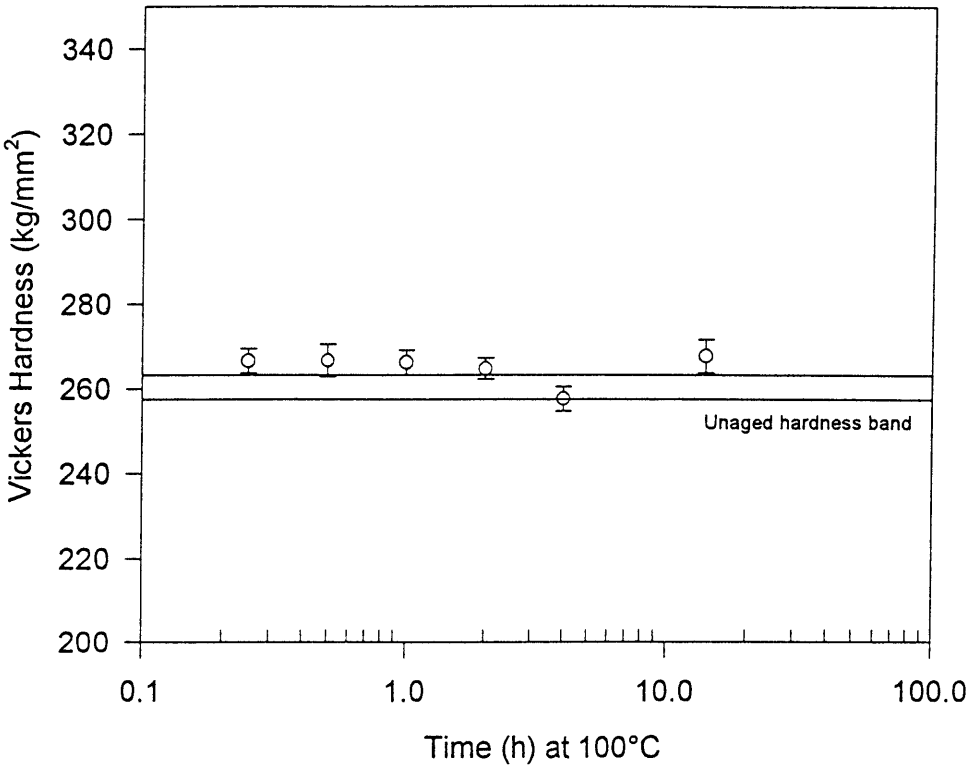

***Figure 4.7**: Hardness of sheet material solution treated at 930℃ (45 minutes), water quenched, cold rolled (38% reduction in area) and aged at 100℃, indicating that no strain aging occurs. 95% confidence intervals are shown*

If strain aging has an effect, it is to be expected that some hardness increase would be evident within the first 12 hours at 100°C. It can clearly be seen that no sign of any significant hardness increase is present even after aging for 64 hours (figures 4.6 and 4.7). It can therefore be concluded that strain aging doen not have a significant effect on the observed aging behaviour. This is consistent with results obtained by others, which reported only a slight increase in hardness after one month at room temperature (Lagneborg 1967).

4.4. Conclusions

Cold working increases the initial hardness of the material substantially. This is probably due to two effects: an increase in hardness directly related to the increased dislocation density; and an increase in hardness because of precipitation processes being promoted by the cold work.

For the present case cold work does not seem to enhance the formation of α", in contrast to previous results (Thielsh 1951, Lena and Hawkes 1954, Tisinai and Samans 1957), as it does not seem to have any other influence on the aging behaviour at longer periods of aging

Strain aging does not play a significant role in the observed strengthening.

With aging some rearrangement of dislocations takes place (recovery), but no recrystallisation is observed.

Chapter 5

The Effect of Aging on the Hardness of Chain Links and Cold-worked 430 (No Prior Solution Treatment)

While chapter 4 considered the effects of cold work, recovery and strain aging on the hardness after aging at 475°C, the hardening mechanism which is most strongly associated with this temperature range is the formation of α". Since α" formation is expected to be strongly temperature dependent, a simple test for the presence of this hardening mechanism can be carried out by aging at temperatures other than 475°C. This chapter presents results on the hardness changes of chain links and cold-worked type 430 sheet material after aging at temperatures from 400°C to 500°C. These results support those of chapter 6, in which Mössbauer results are presented which show that the strengthening obtained after relatively long periods of aging at 475°C is indeed due to the Cr-rich α" phase.

5.1. Aging behaviour

In figure 5.1 the aging curves at 475°C of the chain and sheet material (no solution treatment before cold rolling) are presented. The aging behaviour is similar, as the hardness increases only at longer periods of aging (~ 64 hours) in both cases.

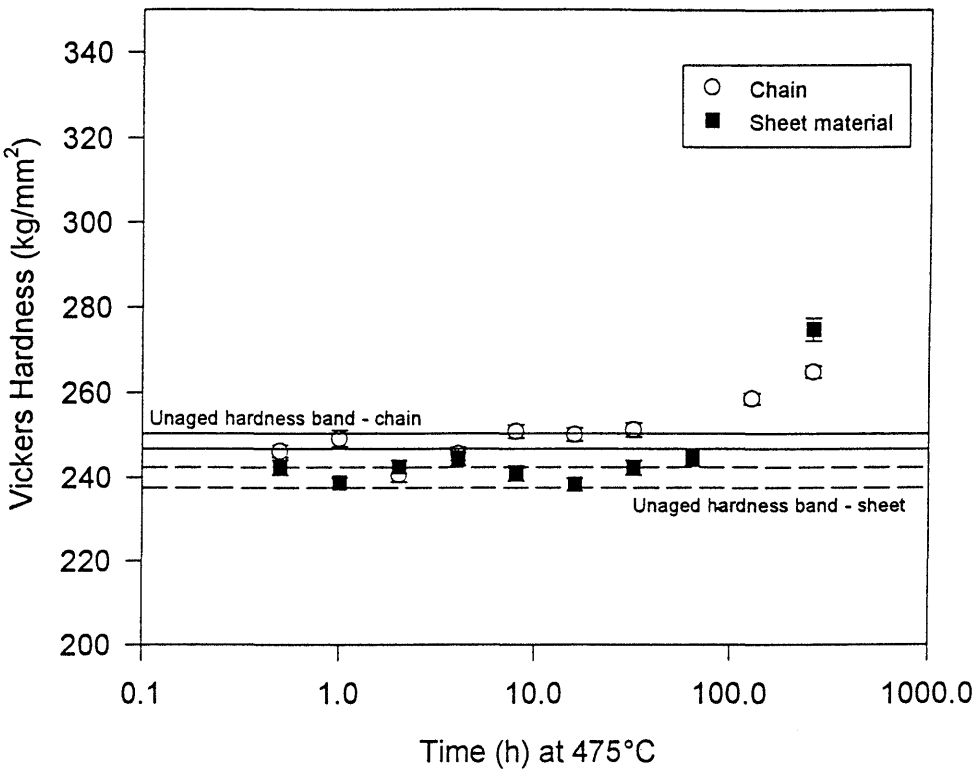

***Figure 5.1**:Hardness of chain links aged at 475 ℃ and of sheet material aged at 475 ℃ (after cold rolling - 38% reduction in area), showing that the aging behaviour of the chain and sheet material are similar*

The initial hardness for the chains is somewhat higher than that of the sheet material, but this is probably due to some martensite in the chain microstructure; investigation of the optical microstructure revealed the presence of two different phases, probably ferrite and some martensite. Martensite may form after annealing above the Ac_1, which - based on the composition as given in table 3.1 - can be estimated to be about 920°C (Pistorius and Coetzee 1996).

The aging behaviour is essentially the same for the curves, both showing an initial "incubation" or plateau region, with a distinct increase in hardness after long aging periods. This increase is most likely due to the precipitation of the Cr-rich α", as supported by Mössbauer results in chapter 6. Although this entails localised Cr depletion, corrosion tests did not reveal any deterioration in general corrosion resistance. It might be that the length scale of the depletion is too small to affect corrosion properties.

To test if the same hardening occurs at temperatures other than 475°C, chain links were also aged at 450°C (figure 5.2); and cold rolled sheet material at 400°C and 500°C (figure 5.3).

The results indicate that the hardening behaviour at 450°C and 475°C is similar, but that no hardening increase is apparent with aging at 500°C. No conclusions can be drawn from the 400°C set as the data points are too limited.

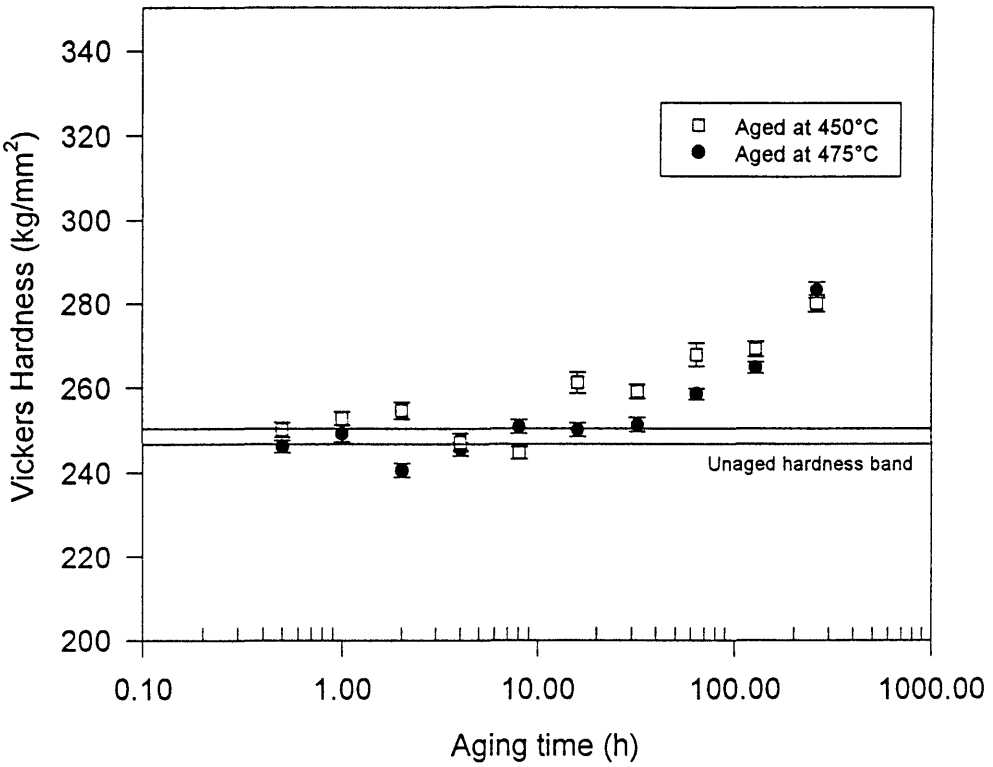

***Figure 5.2**: Hardness of chain links aged at 450℃ and 475℃, indicating that an increase in hardness with long aging periods occur at both temperatures. 95% confidence intervals are shown*

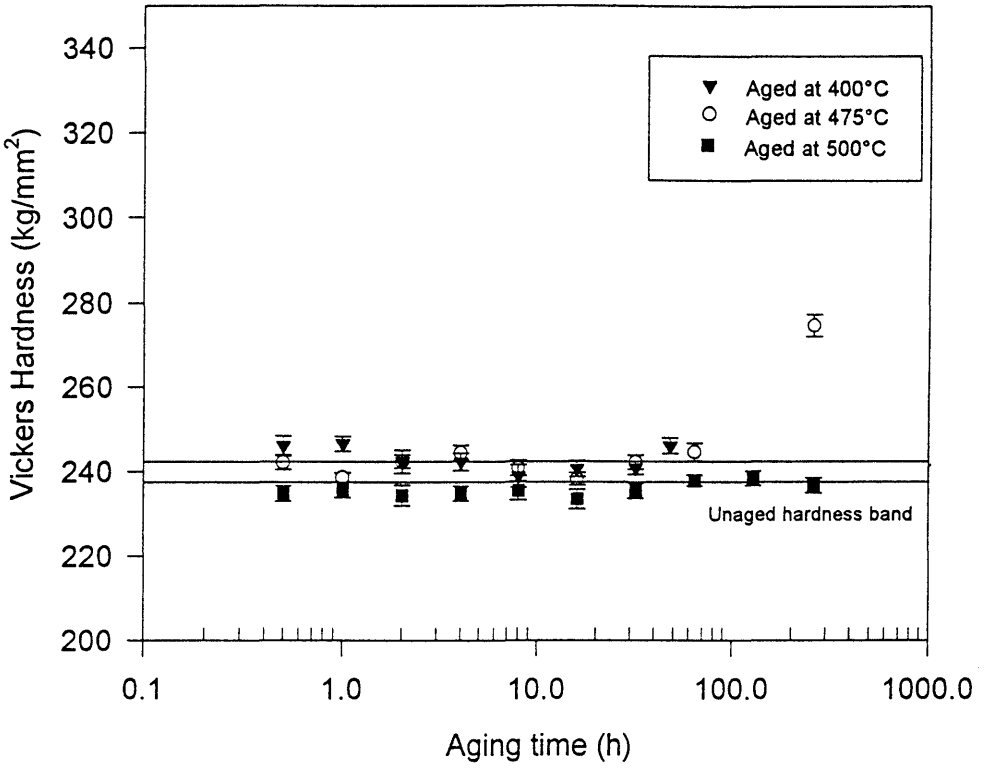

***Figure 5.3**: Hardness of cold rolled sheet material, after aging at 400℃, 475℃ and 500℃, indicating that no hardening occurs after long periods of aging at 500℃. 95% confidence intervals are shown*

The expected equilibrium fractions of α" obtainable at the aging temperatures were determined from the phase diagram (figure 5.4).

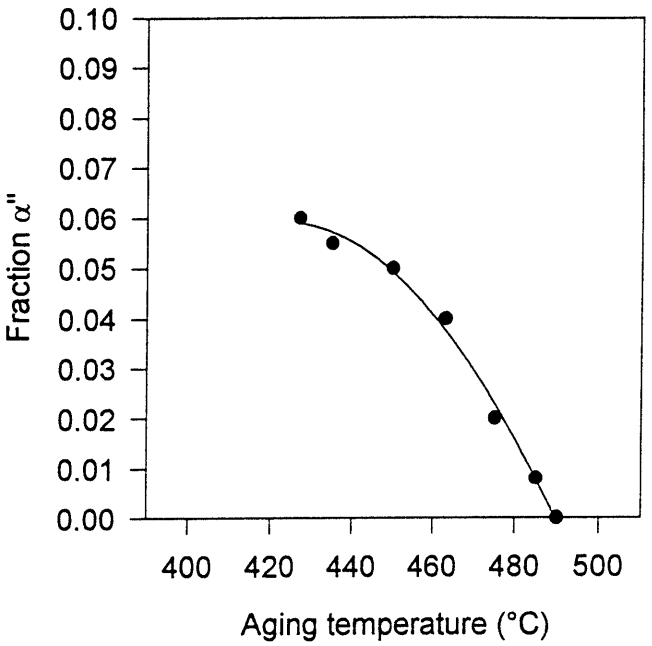

***Figure 5.4**: Expected equilibrium volume fractions of α" in an alloy containing 16.4% Cr at different temperatures as calculated from the thermodynamic assessment of the Fe-Cr-phase diagram by Dubiel and Inden (1987)*

According to the phase diagram the equilibrium fractions of α" at 450°C and 475°C are close enough to expect similar aging behaviour. At this composition (16.4% Cr) aging at 500°C lies outside the miscibility gap and α" is not expected to form - this is confirmed by the fact that the hardness did not increase with aging at that temperature.

The expected two stage behaviour reported by others (chapter 2) was not observed. This is probably due to the low interstitial content of the matrix.

5.2. Conclusions

Aging of the as-received chain (figure 5.1) and cold rolled sheet material (figure 5.2) exhibit the same behaviour - an increase in hardness after approximately 64 hours of aging. This is presumably due to the α" precipitation.

The hardening effect is not present at the higher aging temperature of 500°C, which is consistent with the expected temperature dependence of the equilibrium volume fraction of α".

Chapter 6

The Effect of Solution Treatments on Aging Behaviour

The results of chapter 5 support the suggestion that the hardness increase after aging at 475°C for 64 hours or more results from α" precipitation. If sufficient carbon and nitrogen can be brought in to solid solution, hardening by carbide or nitride precipitation may occur at shorter aging times. The amount of interstitial elements in solution depends on the solution temperature - both because the solubility in ferrite increases with temperature, and because austenite (a carbon and nitrogen sink) forms above the Ac_1 temperature (see figure 2.2). This chapter reports results on experiments which explored the effect of solution treatments on the aging behaviour.

6.1 Determination of Ac_1 temperature

By heating to a sufficiently high temperature, it is possible to enter the three phase ($\alpha+\gamma+M_{23}C_6$) region - as explained in Chapter 2. This boundary ($\alpha+M_{23}C_6 \rightarrow \alpha+\gamma+M_{23}C_6$) is important for subsequent heat treatments; and the temperature at which the transition occurs (the Ac_1 temperature) was determined as follows:

6.1.1. Solution treatments

The start of martensite formation was determined by solution treating 8mm thick samples between 800°C and 1200°C at intervals of 25°C, holding at temperature for 15 minutes, and quenching in water. Additional solution treatment steps were performed with a weld cycle simulator between 900°C and 950°C in steps of 10 degrees (samples held at temperature for 10 minutes). The relatively long holding times ensured that most of the carbon and nitrogen came into solution. The volume fraction of martensite was determined after etching with Ralph's etchant by using a point count method (200 points):

The maximum amount of martensite obtainable with this composition is about 35% at 975°C (figure 6.1). The change in martensite content with temperature reflects how the alloy enters the three phase ($\alpha+\gamma+M_{23}C_6$) and two phase ($\alpha + \gamma$) regions with an increase in temperature, and eventually passes beyond the γ-loop into the single phase (α) region at high temperatures.

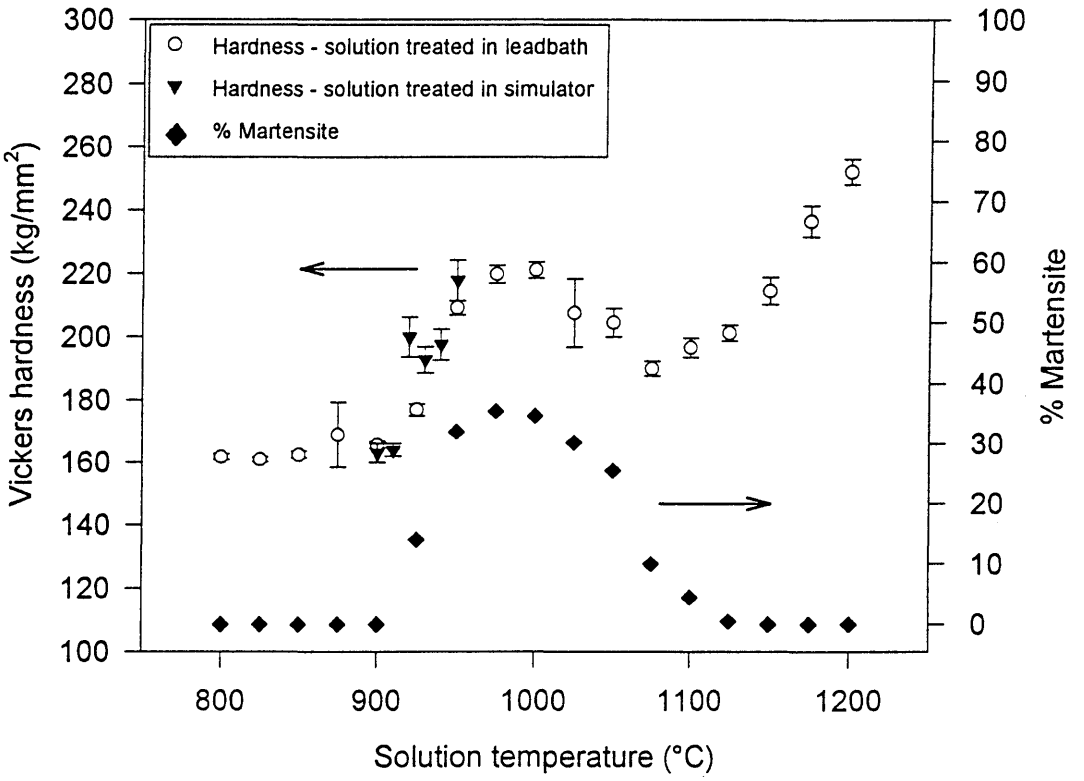

***Figure 6.1**: Vickers Hardness of samples solution treated at different temperatures, followed by quenching in water. A plot of the percentage martensite obtainable at each solution treatment temperature is superimposed on the graph. 95% confidence intervals are shown*

With increasing solution temperatures the distinct increase in hardness coincides with the start of martensite formation. A decrease in hardness can also be seen as the amount of martensite decreases. The second hardness increase (at temperatures higher than 1100°C) is probably due to high temperature embrittlement, in which embrittlement results from a clustering or segregation of carbon atoms in the ferrite matrix, when rapid cooling prevents precipitation of carbon as carbides from solid solution (Demo 1971).

These results indicate that the Ac_1 temperature for this material is approximately 920°C.

6.1.2. The influence of cooling rate after solution treatment

By enhancing the cooling rate through quenching in water (as opposed to air cooling) after solution treatment at 920°C, the hardness could be increased by at least 20 kg/mm^2 over the original hardness (148 kg/mm^2) of the material without damaging the corrosion resistance. This increase in hardness is presumably due to the trapping of carbon and nitrogen in solid solution in the matrix, as the high cooling rate does not allow sufficient diffusion for carbide precipitation to occur. Any effect that the interstitials would have on subsequent aging behaviour would therefore be enhanced by rapid cooling.

Further investigation into the quenching rate revealed that it has a significant effect on mechanical properties. This was established by quenching in water and in brine (2% NaCl) after solution heat treatment at 930°C (annealing). The test sample was 170×70×8 mm in size and the temperature of the specimen was measured by inserting a thermocouple approximately 1 cm into the side of the specimen (figure 6.2).

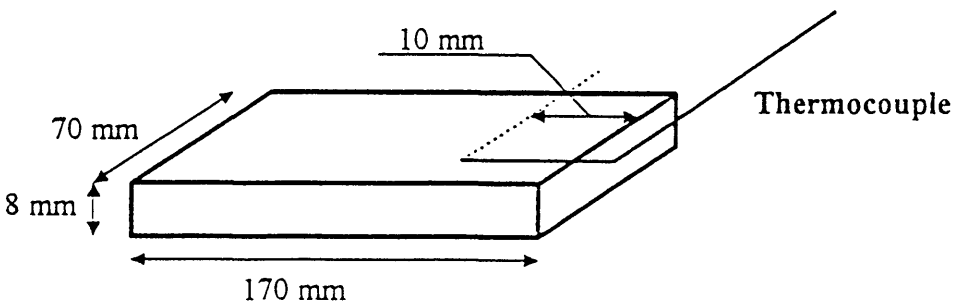

***Figure 6.2**: Configuration of test specimen and thermocouple to determine cooling rates*

Quenching in the brine resulted in a faster cooling rate (650°C/s in a 2% NaCl solution and 160°C/s in water), as the added ions in the brine accelerate boiling of the quenching liquid, thus eliminating any effect a vapour blanket would have on the cooling (Bates *et al.* 1991).

The quenching rate - which is affected by variations in the quenchant temperature and composition - influences the hardness by as much as 23 kg/mm^2 (samples 170×70×8mm in size). This is probably due to the amount of carbon and nitrogen that could be trapped in solution. It was established through aging experiments that the difference in initial hardness does not affect the strengthening *trends*, thus if the strengthening *mechanism* is studied, small variations in quenching conditions are not thought to be of great importance. However, in practical applications (where the absolute hardness, rather than hardness changes, is to be controlled) maintenance of consistent cooling conditions will clearly be crucial.

All solution heat treatments, with the exception of those performed in the weld simulator, were followed by quenching in brine (approximately 2% NaCl)

6.2. Choice of acceptable solution temperatures

Based on the experimentally determined Ac_1 temperature, two solution temperatures were selected for further experiments, one below and one above the Ac_1.

6.2.1. Solution temperature below the Ac_1 temperature

880°C was decided upon as it is within the range of the annealing temperatures used in industry (J. Hewitt, personal communication).

6.2.2. Solution temperature above the Ac_1 temperature

As it had been reported that the addition of martensite to the microstructure increases strength to the extent that the requirements set for conveyor applications could easily be met, the influence of the martensite on aging behaviour was investigated. In order to accomplish that a temperature higher than the Ac_1 had to be selected. As the Ac_1 temperature was established to be approximately 920°C, the selected temperatures were 930°C and 990°C. After the solution treatments the material was cold rolled (38% reduction in area) and subsequently aged at 475°C.

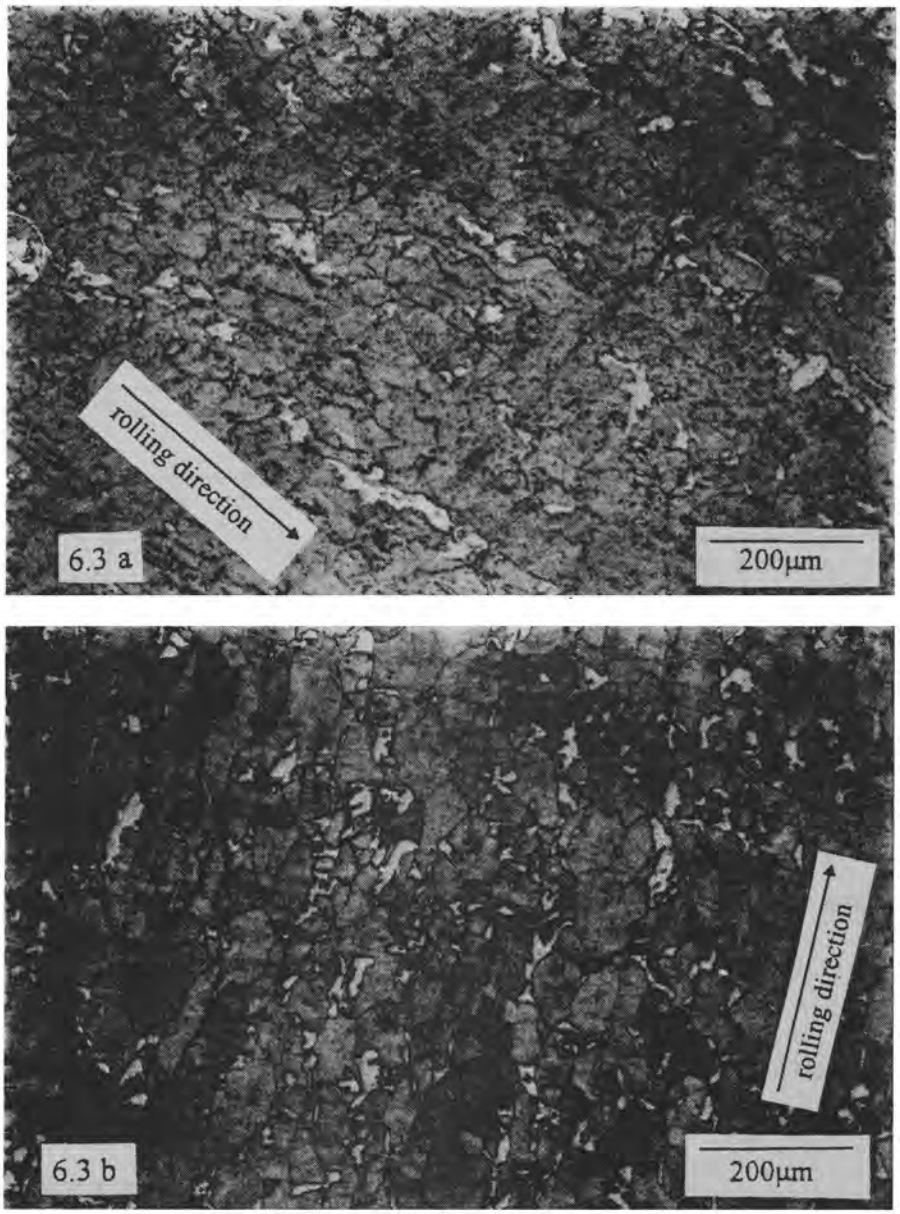

***Figure 6.3**: Microstructures after solution treatment (15 min) at (a) 930℃ (showing ferrite, martensite and carbides) and (b) 990℃ (showing ferrite and martensite)*

The microstructure contains three phases after solution treatment at 930°C; these are ferrite (grey phase), some martensite (white phase) and carbides (black dots). A duplex ferrite-martensite structure results after solution treatment at 990°C.

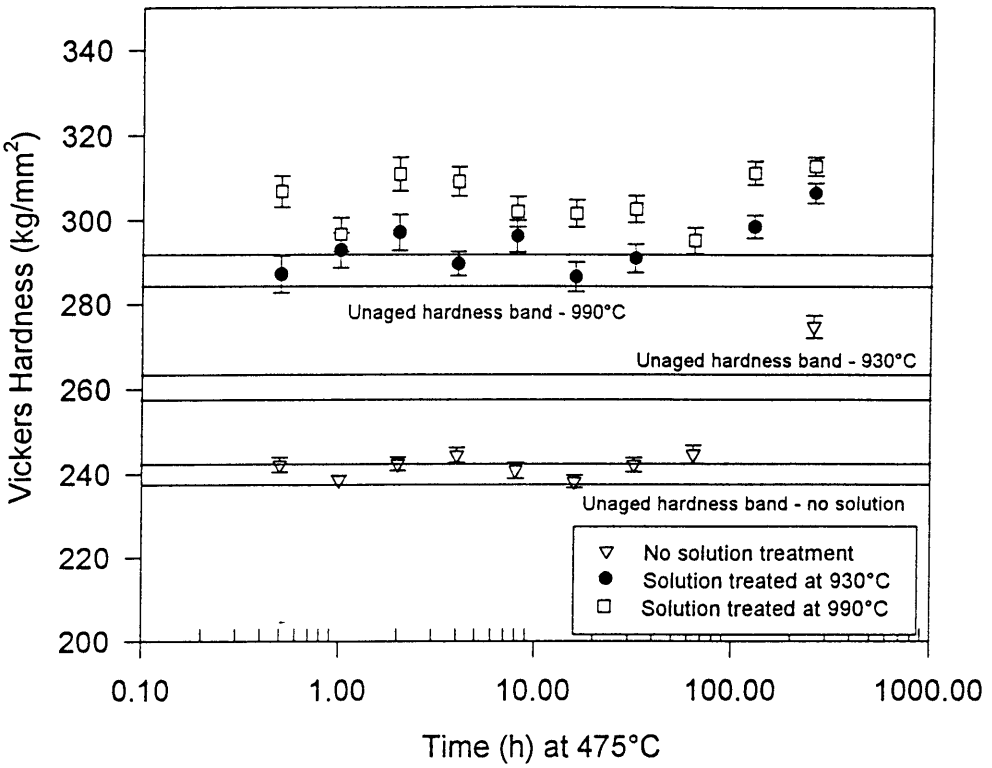

***Figure 6.4**: Hardness after aging at 475℃. Samples were solution treated at 930℃ and 990℃ respectively before cold rolling and aging. For comparison the curve of the material not solution treated is included. 95% confidence intervals are shown*

The hardness curves indicate that the additional solution treatments provide a marked increase in hardness. This is probably due to the increased carbon and nitrogen content as well as the presence of martensite caused by the high solution temperature.

It is also revealed that, although the initial hardness values differ markedly for the two solution treatments, the aging behaviour of the two treatments are similar; in addition, the difference in hardness diminishes at extended periods of aging.

For practical reasons - the temperature being sufficiently close to the present annealing temperature, and thus more easily attainable - the lower solution temperature (930°C) was selected for the subsequent investigation.

6.3. Effect of solution treatments on aging behaviour

6.3.1. Solution treatment at 880°C and 930°C and aging at 475°C

The material (in the form of specimens approximately 170×70×8 mm in size) was solution treated at 880°C and 930°C respectively, in an air furnace for 30 minutes, after which they were quenched in brine (approximately 2% salt) and cold rolled (a 38% reduction in area). Smaller pieces (about 20x20×5mm) were aged in a lead bath at 475°C for 0.5h to 2072 hours, while other samples (15x70×5mm) were aged in the weld cycle simulator where the short holding times could be controlled accurately.

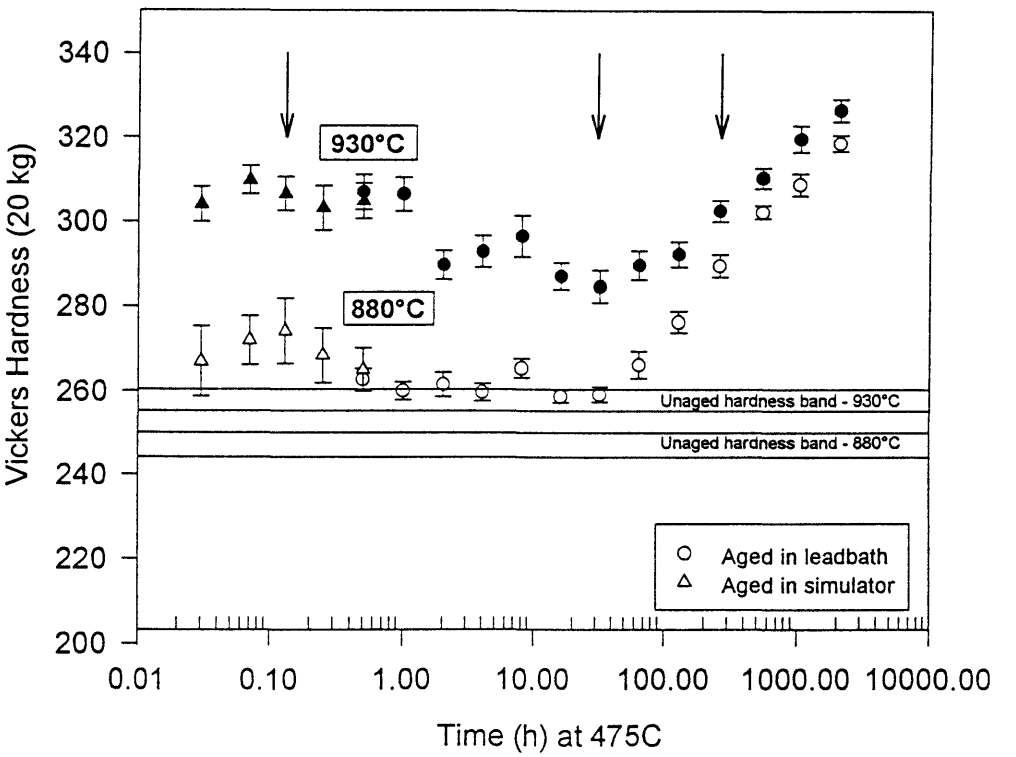

***Figure 6.5**: Hardness of samples solution treated at 880℃ and 930℃, cold rolled and aged at 475℃. 95% confidence intervals are shown. Arrows indicate specimens selected for further examination by TEM and Mössbauer spectroscopy, as well as mechanical testing*

Solution treatment at the higher temperature (930°C) increases the initial Vickers hardness by 10 kg/mm^2 from 247 kg/mm^2 (figure 6.5). However, during the first stages of aging the difference increases beyond this. In both cases a peak can be observed after only 8 minutes of

aging. For the 880°C samples there seems to be an immediate decrease in hardness after this peak, while somewhat of a plateau is present for the 930°C samples. Other authors also noted three stages in hardness with aging in this temperature region. The first stage, however, was not so pronounced (Nichol *et al.* 1980).

This peak in hardness is most likely caused by the precipitation of coherent carbides and nitrides. These seem to be rich in chromium, as Mössbauer studies indicate a Cr depletion of the matrix (section 6.4.2). These precipitates are also expected to be very fine but dispersed throughout the grains and not concentrated at the grain boundaries (Pednekar and Smialowska 1980). The decrease in hardness following this peak is probably associated with overaging, where coherency is lost (Dieter 1988, p. 213) or Ostwald ripening occurs.

For specimens subjected to both solution treatments, the hardness again increases for aging beyond 64 hours. This point possibly indicates the starting of α" formation.

It seems that by aging for only 8 minutes or for more than 22 days the same increase in hardness can be obtained. This has important practical implications for manufacturing and strengthening treatments.

There is no indication of overaging at periods where the α" is the main strengthening mechanism ($t > 64$ hours) in either curve: the material displayed a sustained increase in hardness with aging time. The initial hardness increase is much higher for the 930°C solution treatment, but at very long periods of aging the two curves tend to converge (see 2072 hours). This effect may be explained qualitatively, based on microstructural changes.

The microstructure of the 880°C solution treated sample did not change markedly with aging (figure 6.6(b)) from the initial structure (figure 6.6(a)). The 930°C solution sample, however, show distinct changes in structure: as can be seen in figure 6.7(b), the martensite has the appearance of being tempered. As the martensite is tempered it becomes softer and hence the additional strengthening is lost. Tempering will eventually convert the martensite to ferrite and $(Cr,Fe)_{23}C_7$-carbides (Brooks 1979, p. 186). The softening effect of tempering is also a

plausible explanation for the larger hardness decrease for the martensite containing material, for aging beyond 8 minutes.

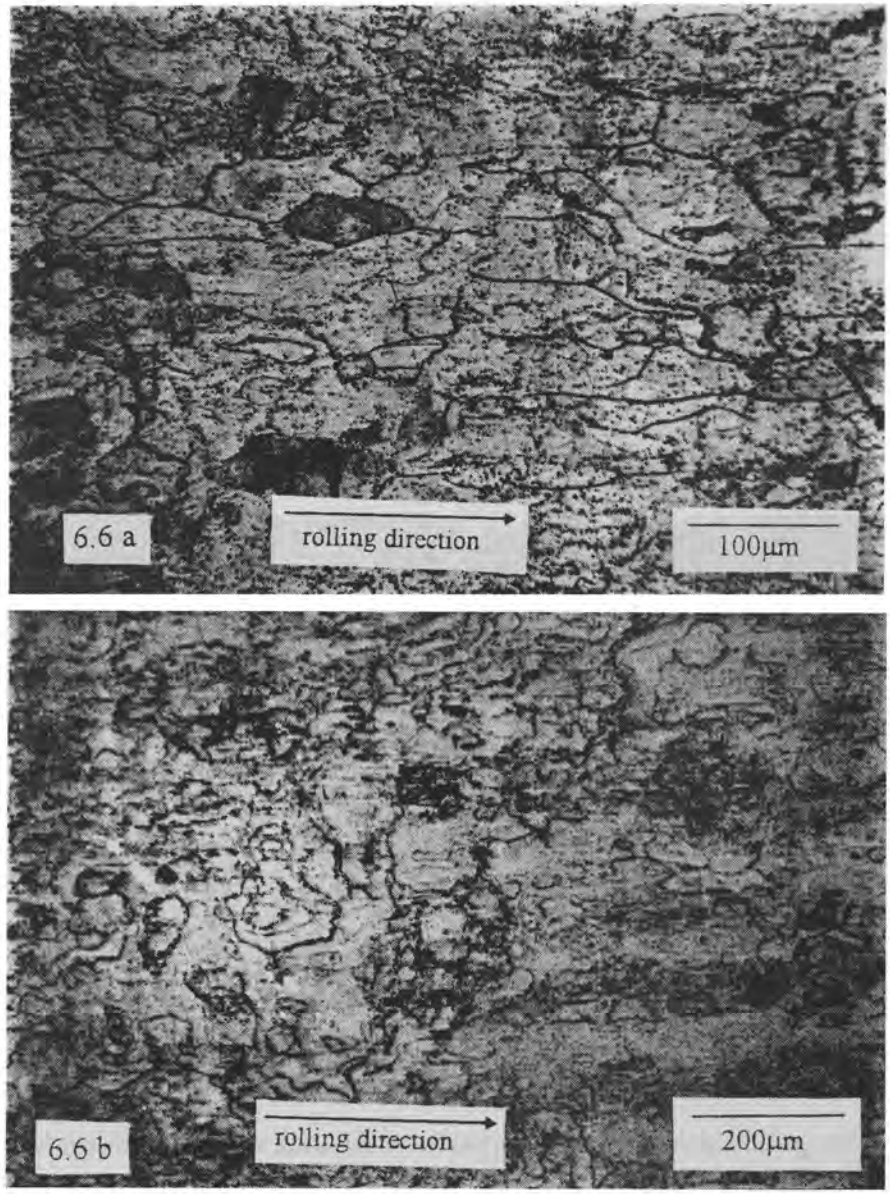

Figure 6.6: *Microstructure after solution treatment at 880℃ and cold rolling (38% reduction), (a) before aging and (b) after aging at 475℃ for 2072 hours*

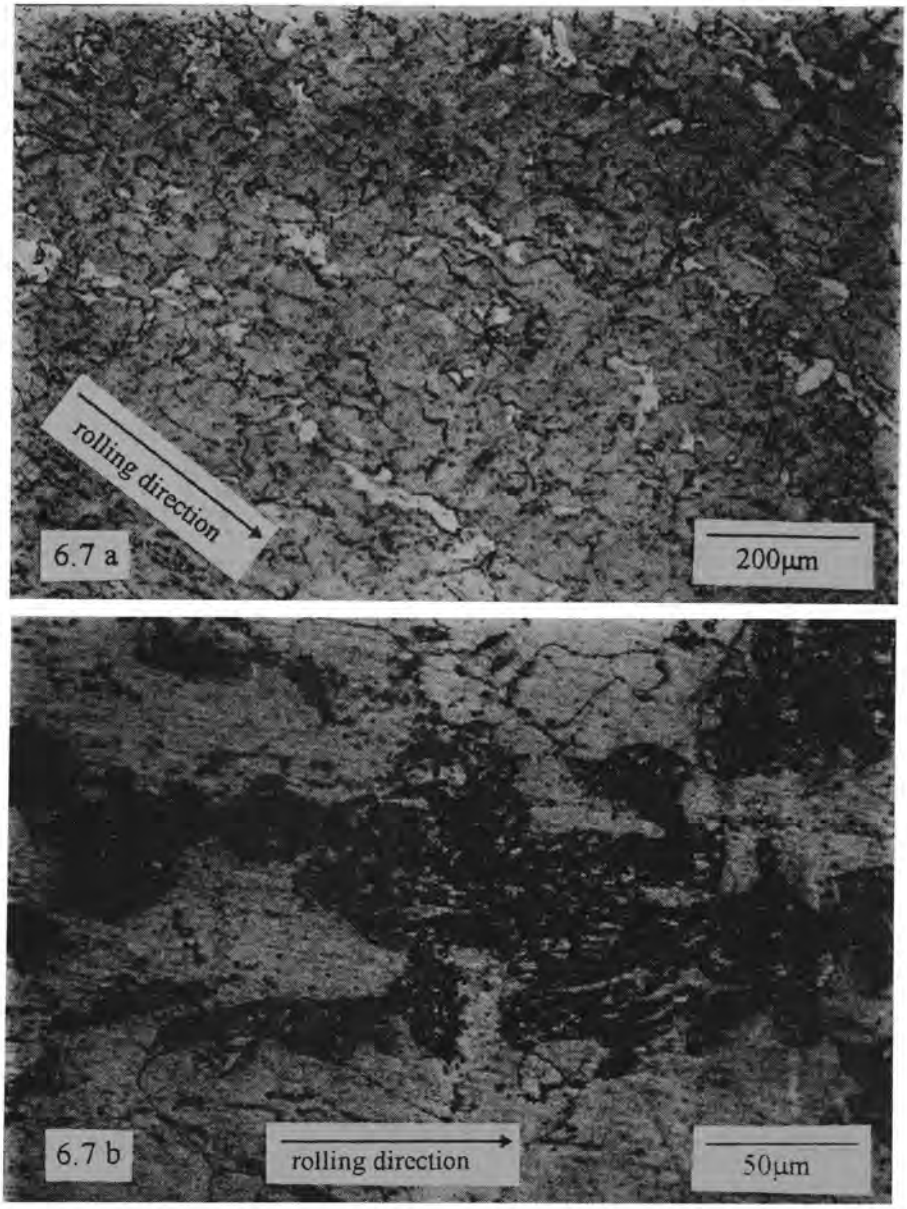

Figure 6.7: *Microstructure after solution treatment at 930 ℃ and cold rolling (a) before aging; and (b)after aging at 475 ℃ for2072 hours*

The effect of α" formation only becomes apparent after aging for approximately 64 hours. This is the case for specimens that had been solution treated before cold rolling and aging (figure 6.5), as well as those that had not been given an additional solution treatment (figure 5.3). The difference between the two solution treatments is only apparent in the short-time aging behaviour (in this case < 64 hours), hence it could be argued that in this case the additional solution treatments only have an influence on strengthening mechanisms based on the effect of carbon and/or nitrogen and that the formation of α" is not affected.

6.3.2. Solution treatment at 880°C and 930°C, and aging at 450°C

Results presented in section 5.1 indicated that hardening also occurs readily with aging at 450°C (figure 5.2). This investigation was therefore extended to the lower temperature to determine whether the aging behaviour would be similar to that at 475°C, with solution treatments prior to cold rolling and aging.

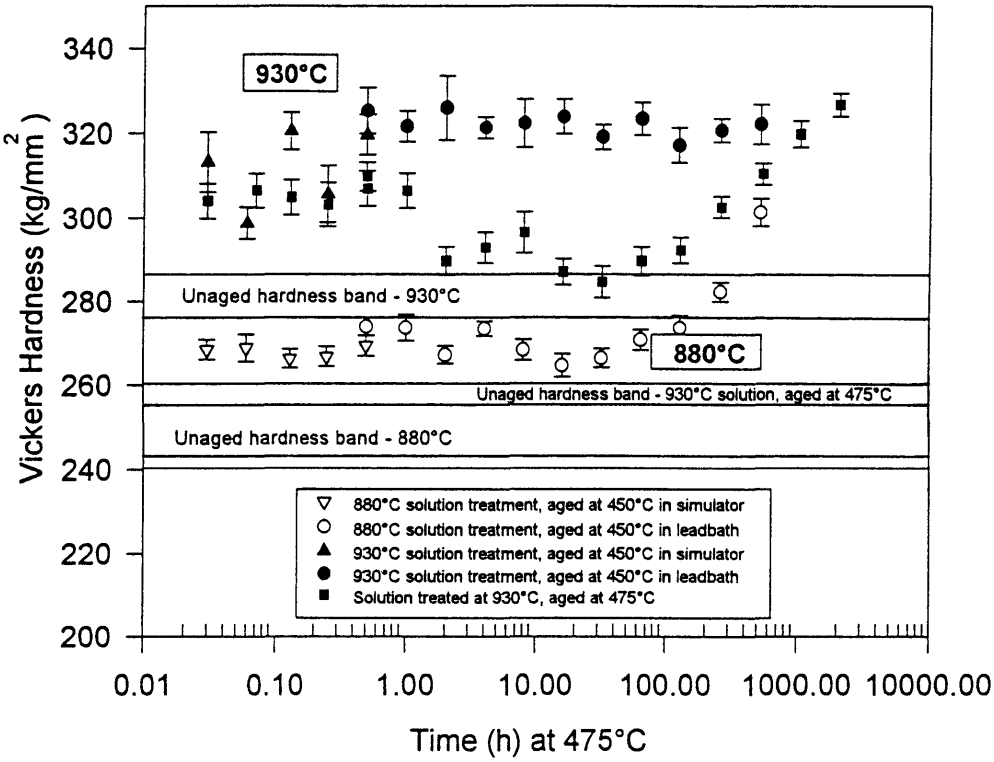

***Figure 6.8**: Hardness after solution treatment at 880 ℃ and 930 ℃, cold rolling and aging at 450 ℃. The curve for aging at 475 ℃ (solution treatment at 930 ℃ and cold rolling) is also plotted, indicating overaging at the higher aging temperature. 95% confidence intervals are shown*

The hardening behaviour is similar for aging at both 450°C and 475°C for the samples solution treated at 880°C. The hardness increase is not the same for the corresponding 930°C solution treated samples, however. When aged at 450°C a hardness increase of about 37 kg/mm^2 is observed, while with aging at 475°C an increase of 46 kg/mm^2 is noticed. This effect might be more pronounced because of the big variance in initial/unaged hardness of the two sets of solution treatments at 930°C, resulting from a difference in quenching conditions.

There does not seem to be the same decrease in hardness as experienced with aging at 475°C, which is associated with overaging. It is thought that overaging of the precipitates does not occur because of the somewhat lower diffusion rates at this lower aging temperature (450°C).

In the 880°C solution treated samples there is again the increase in hardness after longer aging times (>32 hours). No comment can be made about the 930°C results as it is not clear whether hardness would increase with longer aging, although from the phase diagram α" is expected to be present.

6.4. Strengthening mechanisms

The results obtained so far are consistent with observations previously reported for ferritic stainless steels aged around 475°C, namely that short-time strengthening is caused by the precipitation of Cr-rich (cf. section 6.4.2) carbides and/or nitrides, while after some incubation period, α" causes strengthening. It was considered useful to launch a detailed investigation of selected aging periods to elucidate the mechanisms causing strengthening, as well as the influence on mechanical properties (discussed in chapter 7). The periods that were selected are: 8 minutes, which coincides with the point of maximum hardness for short aging periods; 32 hours, which represent the point just before α" seems to have an effect; and 260 hours which should be well within the α" region (indicated by arrows on figure 6.5).

6.4.1. Carbide and nitride precipitates

With the aid of transmission electron microscopy it was possible to identify precipitates of sizes in the order of 1 μm. The precipitates varied from spherical to almost perfect rectangular in form. Through their diffraction patterns they were identified as $M_{23}C_6$ with M = FeCr. The camera constant was determined to be 6.07×10^{-12} through measuring the known diffraction pattern of the α matrix.

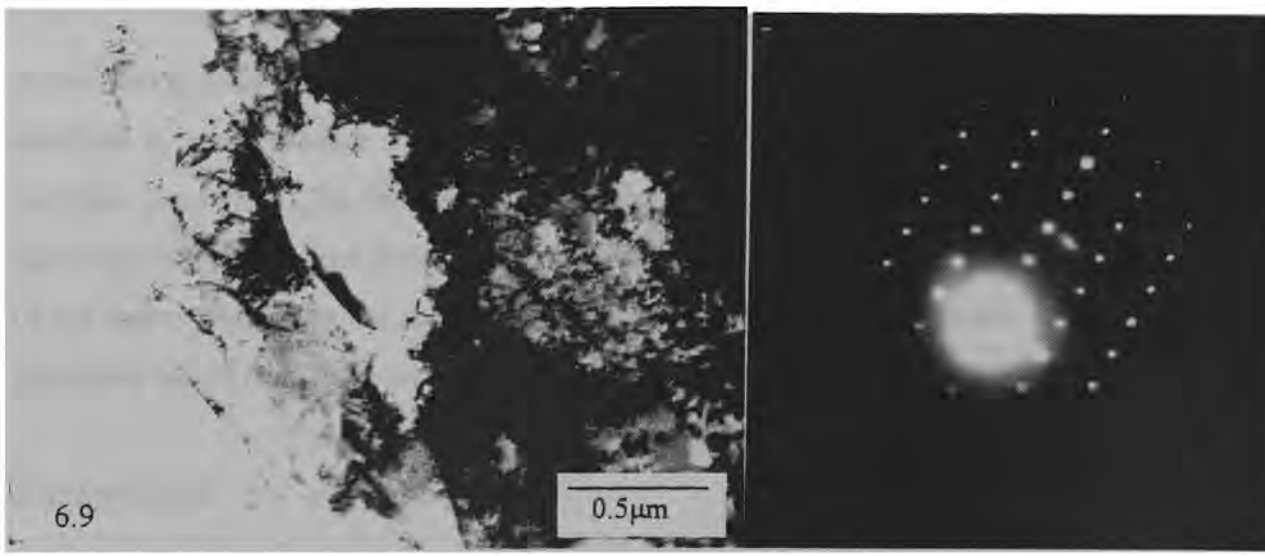

***Figure 6.9**: TEM micrograph of precipitate and selected diffraction pattern (sample solution treated at 930 ℃ and aged for 260 hours at 475 ℃)*

The precipitates were frequently situated on grain boundaries, but sometimes they formed rows in seemingly clear areas. This could indicate that precipitates formed on original grain boundaries or that the grain boundaries were pinned by the precipitates. The relative large sizes of the precipitates, along with the fact that precipitates could be detected in the unaged condition, suggest that these precipitates were present in the original sheet material, and that they are not the precipitates causing strengthening.

It seems very likely, however, that the precipitation of essentially Cr-rich carbides and nitrides are responsible for the initial increase in hardness (figure 6.5), as it has been found that a dramatic decline in toughness and increase in hardness occur before precipitates can be observed. It is suggested that the effects on mechanical properties are due to residual C and N in the matrix, perhaps in the form of extremely small Cr-C or Cr-N clusters (Grobner 1973, Cortie 1995).

No traces of the α" precipitate could be found by transmission electron microscopy. However, Mössbauer spectroscopy was used to detect the α", as described in the following section.

6.4.2. α" precipitate

A tool that is useful for the detection of the α" precipitates is Mössbauer spectroscopy as it is sensitive to small changes in the microstructure and is specifically sensitive to the local magnetic properties. The detection of α" is therefore possible as the α", being Cr-rich, is paramagnetic, whereas the ferrite matrix is ferromagnetic. In addition the magnetic properties of the matrix depend on the amount of Cr in solid solution, hence changes in the magnetic properties can be used to deduce information on the formation of Cr-rich precipitates.

Background

Mössbauer spectroscopy involves bombarding a target with a stream of gamma-rays; small shifts in the energies of the transmitted rays are obtained in the Mössbauer apparatus as a result of the Doppler principle. This is achieved by moving the source and sample relative to one another. The Mössbauer spectra are normally given as plots of absorption against relative velocity (in mm/s). The absorption characteristics are affected by the electronic environment of the nucleus, producing the hyperfine interactions (Czakó-Nagy and Vertés 1988).

The principal hyperfine parameters derived from the Mössbauer spectrum are the hyperfine field, isomer shift and quadrupole splitting.

The splitting of the nuclear energy levels in a magnetic field produces transitions that are each seen as a line in the Mössbauer spectrum. The energy difference between the first and last lines is directly related to the effective magnetic field experienced by the nucleus. This gives rise to the hyperfine field.

The isomer shift arises from the fact that the electron density near the nucleus varies with the chemical state of that nucleus. Thus the position of the resonance absorption peak depends on the chemical environment of the atom.

The charges distributed asymmetrically around the atomic nucleus (electrons, ions and dipoles) result in an electric field gradient that is not equal to zero at the site of the atomic nucleus. The

interaction of this electric field and the quadrupole moment of the atomic nucleus results in the splitting of the energy levels. The energy difference between the quadrupole split levels is known as the quadrupole splitting.

The effect of the principal hyperfine interactions on the 57Fe (the only iron isotope that shows the Mössbauer effect) spectrum can be seen in figure 6.10:

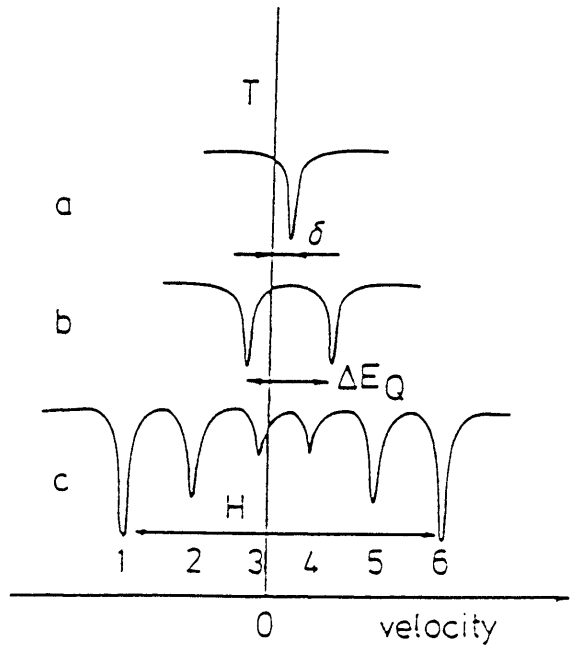

***Figure 6.10**: The effect of the principal hyperfine interactions. (a) isomer shift, (b) quadrupole splitting and (c) hyperfine field (Czakó-Nagy and Vertés 1988)*

Aging

Specimens solution treated at 880°C and 930°C, as well as those without additional solution treatment, were aged at 475°C for different periods. Their Mössbauer spectra and hyperfine parameters were determined.

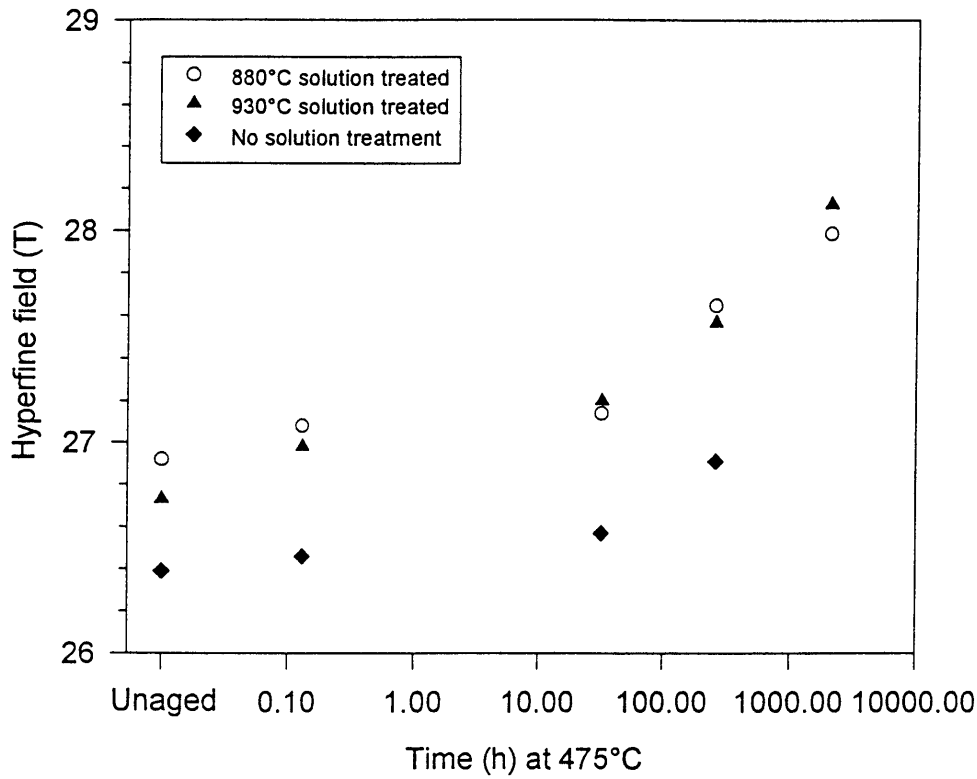

***Figure 6.11**: Distribution of hyperfine field with aging time at 475 ℃, the increase in the field indicates that chromium is removed from the matrix*

The increase of the hyperfine field (figure 6.11) indicates that parts of the matrix become enriched in iron, and by implication, others in chromium. The change in hyperfine field of the solution treated specimens for the period 0 to 8 minutes, is more than double that of the untreated one for the same time period. This increase is most likely caused by the precipitation of Cr-rich carbides and nitrides in the solution treated specimens: the hyperfine field increases as the Cr content of the matrix is lowered. The increase in the field after 32 hours of aging is probably due to α" precipitation. The trend exhibited by the hyperfine field is in good accord with that of the hardness values, namely an initial increase, followed by a second one at longer periods of aging.

That there is some change in composition with aging is verified by the fact that there is a slight increase in magnetic field as aging progresses. This is indicated by a shift to higher velocities of the Fe-sextet (outward expansion), without any paramagnetic effects influencing the profiles. This expansion is characteristic of decomposition via the process of nucleation and growth of a Cr-rich precipitate (Chandra and Schwartz 1971).

It was shown that α" does form at this composition and aging temperature - but this is only clearly evident after very long (approximately 3 months) aging periods (Figure 6.12).

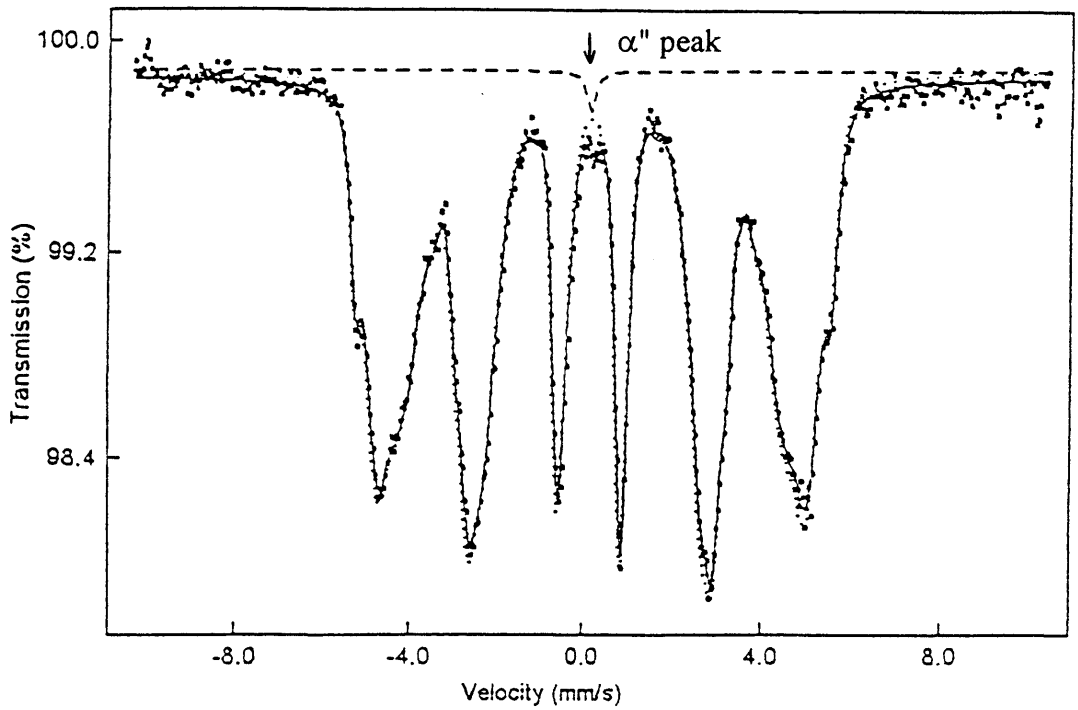

***Figure 6.12**: Mössbauer spectrum of 930 ℃ solution treated sample, cold worked and aged at 475 ℃ for 2072 hours, showing the paramagnetic peak of α" at zero velocity*

The six peaks are characteristic of α-Fe (Chandra and Schwartz 1971, Gonser 1983, Montano 1986) and the presence of the α" is indicated by the peak at 0 velocity, arising from the paramagnetic contribution of the chromium-rich phase.

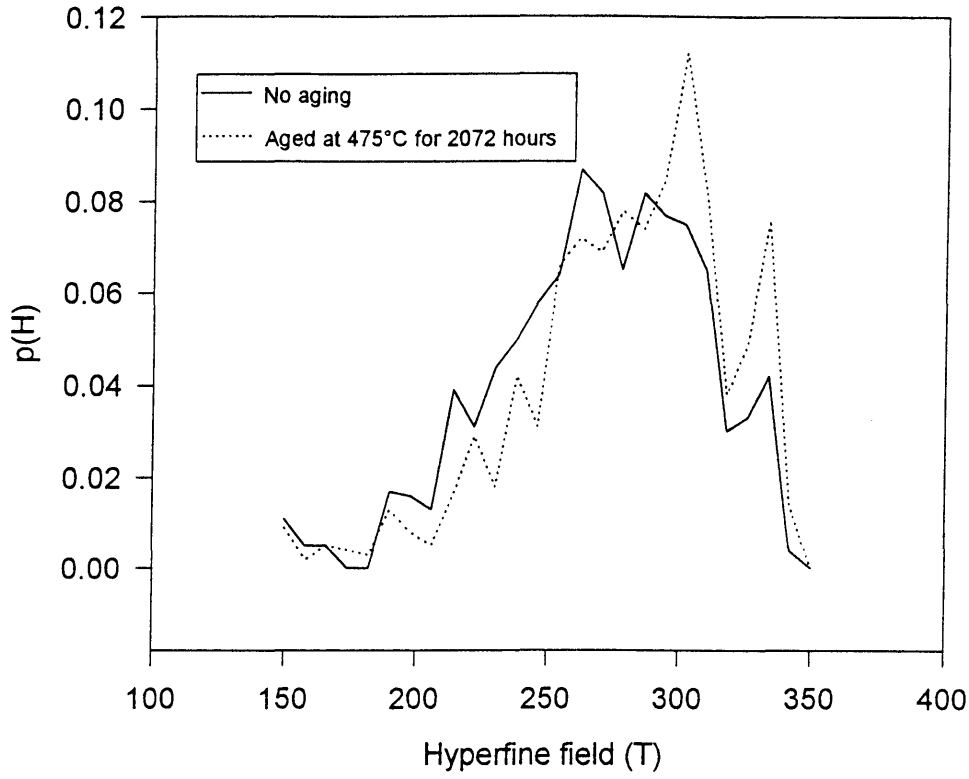

***Figure 6.13**: Field distribution of 880 ℃ solution treated specimens, showing the shift to higher values of the hyperfine field after 2072 hours at 475 ℃*

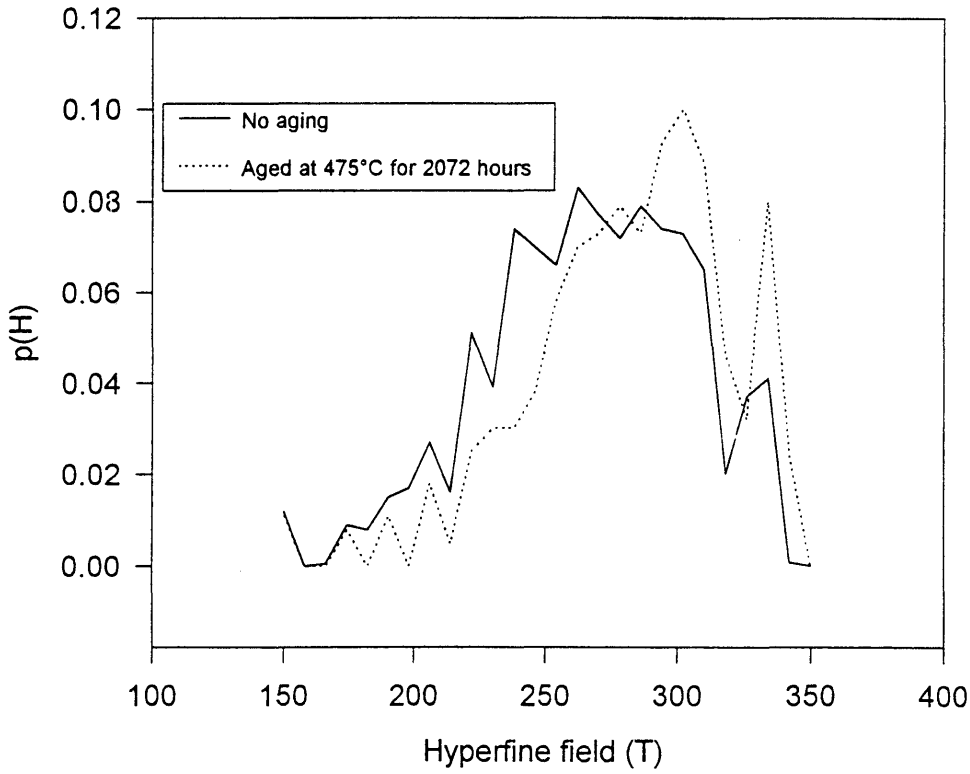

***Figure 6.14**: Field distribution of 930 ℃ solution treated specimens. Before aging and after 2072 hours at 475 ℃, indicating shift to higher hyperfine field values after aging*

The displacement of the p(H) curves to higher values of the hyperfine field without broadening of the distributions (figures 6.13 and 6.14) confirms that the α" is formed through nucleation and growth of particles having the equilibrium composition (Trindade and Vilar 1991), rather than by spinodal decomposition.

It can be concluded that α" precipitation definitely occurs and α" formation is thus assumed to contribute to the strengthening, albeit only at longer aging periods. The precipitates (α") can only be detected after very long periods of aging (for this composition and aging temperature), when the volume fractions of the Cr-rich clusters have become large enough for detection.

6.5. Conclusions

Two stages can be distinguished in the aging behaviour if additional solution treatments are performed before cold rolling and aging. An initial increase in hardness at short aging periods can be observed, which is attributed to the precipitation of Cr-carbides and nitrides, and a second increase at long periods of aging due to the formation of α".

Solution treatments enhance the precipitation of carbides (and nitrides) and cause a subsequent increase in hardness, but do not markedly influence the kinetics of α" formation; the precipitation of α" seems to become appreciable only after 64 hours of aging, regardless of treatment before cold rolling and aging.

Solution treatment at 920°C (higher than the Ac_1) introduces martensite into the structure, which raises the initial, unaged hardness, but does not seem to affect the overall aging behaviour.

With aging at 475°C a decrease in hardness is observed before the formation of α"; this is probably caused by overaging of the carbides and nitrides. No overaging occurred at 450°C, possibly because of the lower diffusion rates.

The α" is formed through the process of nucleation and growth. This is confirmed by the increase in magnetic field as well as the displacement of p(H) curves to higher hyperfine field values.

Chapter 7

Effect of Cold Rolling and Heat Treatments on Mechanical Properties

Chapters four to six presented the hardening that could be obtained by solution heat treatment, cold rolling and aging (primarily at 475°C). Hardness is a convenient way of measuring strength - the reason for its use in the previous chapters - but in actual use the chains are exposed to both tensile and impact loading. Therefore the strength (represented by the yield stress) and the fracture toughness are more applicable mechanical properties. In this chapter the effect of the treatments on properties such as impact strength, fracture toughness, tensile and yield stress and work hardening rate is investigated, while their effect on corrosion resistance is presented in the following chapter.

7.1. Impact strength

Impact tests were performed on specimens solution heat treated at 880°C and 930°C, cold rolled (38% reduction in area) and aged at 475°C for 8 minutes and 32 hours. Unaged samples were also tested. Four sub-size specimens were tested in each condition, having the dimensions given in figure 3.2. Tests were performed at ambient temperature.

The results presented in figure 7.1 indicate that a marked drop in impact strength occurs after only 8 minutes of aging, but that there is not a significant difference in impact strength with aging from 8 minutes to 32 hours.

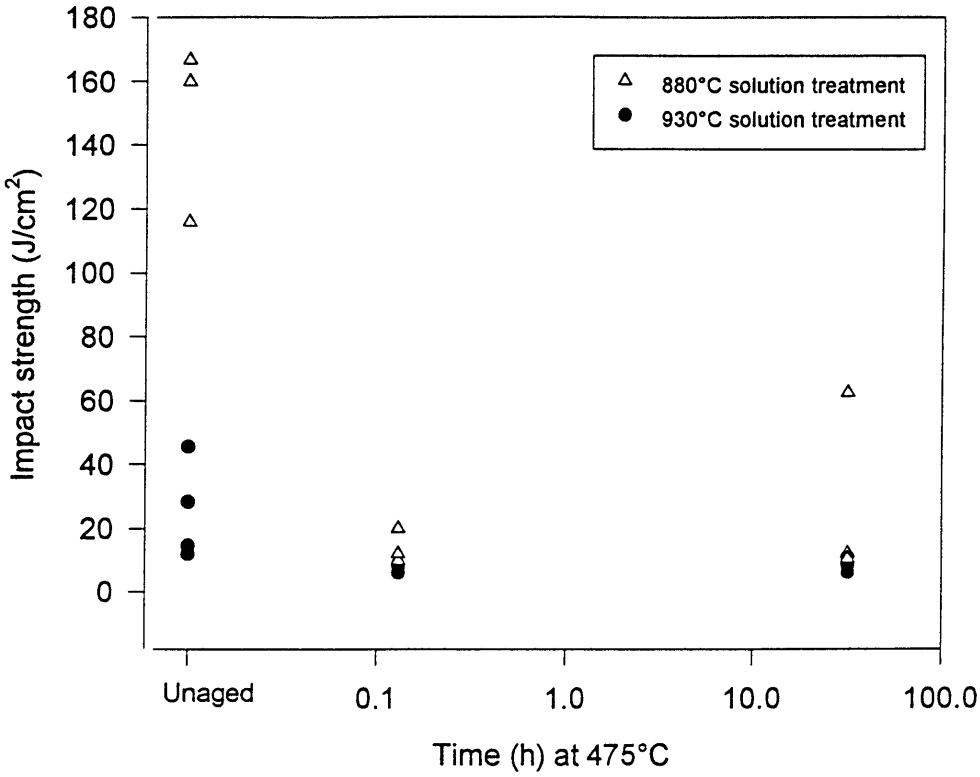

***Figure 7.1**: Impact strength of specimens (55×10×5 mm in size) aged at 475℃, after solution treatment (at 880℃ and 930℃ respectively), and cold rolling. Testing performed at ambient temperature. The results indicate a marked decrease in toughness after 8 minutes of aging*

The lateral expansion of the specimens was determined by measuring the compression side of the impact specimen with a micrometer, and calculating the difference between the initial size (L_i) and expanded size (L_e) as a percentage of the initial size, i.e. $(L_e-L_i)/L_i \times 100$. Like the amount of energy absorbed, the lateral expansion can be used to evaluate the impact resistance - the greater the expansion, the more plastic deformation (and hence energy absorption) before fracture (Rolfe and Barsom 1977, pp. 199-204).

A similar trend, as with the impact strength, is exhibited by the lateral expansion of the specimens (figure 7.2), namely a dramatic decrease in expansion, as aging proceeds.

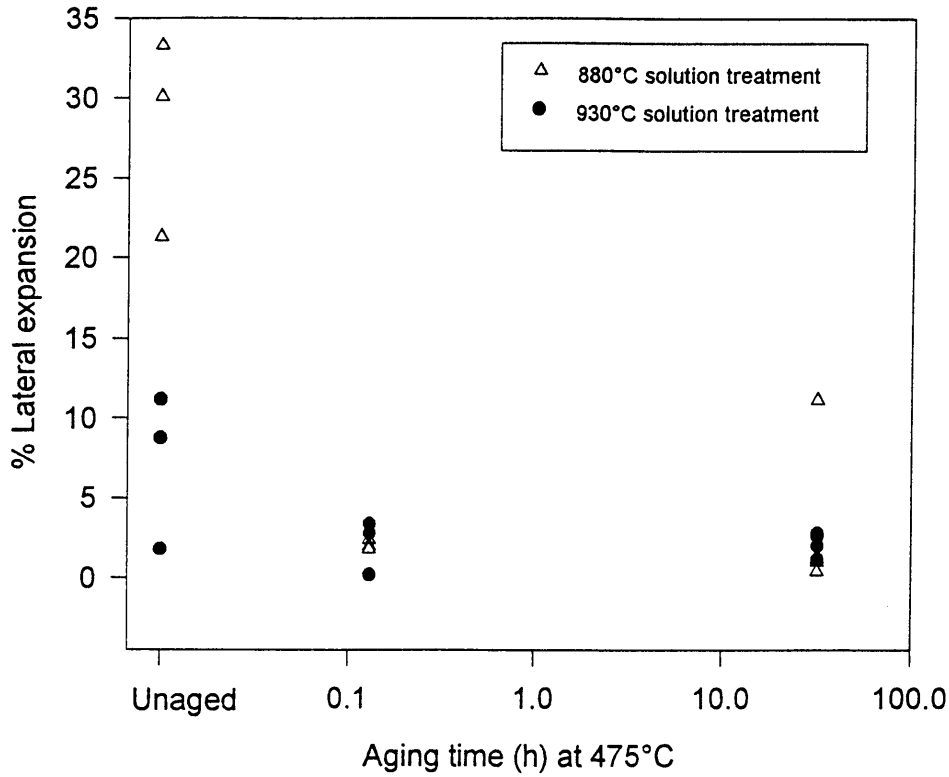

***Figure 7.2**: Lateral expansion of impact specimens, aged at 475℃; after solution treatment at 880℃ and 930℃ and cold rolling. Results show a decrease in % expansion as aging proceeds, indicating a loss in ductility*

Both the impact strength and lateral expansion indicate that embrittlement accompanies the increased hardness obtained by aging. However, these values, as such, do not give an indication of the practical implication of the embrittlement. In this respect the fracture toughness (K_{Ic}) is a more useful property.

Local stresses near a crack depend on the product of the nominal stress and the square root of the half-flaw length. This relationship is quantified by the stress intensity (K). There are several modes of deformation that could be applied to a crack, one of which is known as Mode I, where a tensile stress is applied normal to the faces of the crack. This is the usual mode for fracture-toughness tests and a critical value for stress intensity for this mode would be denoted K_{Ic}. K_{Ic} values are valid material properties, independent of specimen thickness (Dieter 1988 p.351-355).

From the impact strength it is possible to estimate K_{Ic} values. The following equation, linking the CVN values and K_{Ic}, was used:

$$K_{Ic} = 6.79\ (\text{CVN})^{0.75} \qquad (7.1)$$

with K_{Ic} in MPa $(\text{m})^{0.5}$

CVN in J/cm^2

Equation 7.1 can be used for ferritic steels having a yield stress between 270 and 1700 MPa, and an impact range of 14 - 82 J (Hertzberg 1983). The properties of the material investigated here mostly fall into these ranges.

Once the K_{Ic} values are known, it is possible to determine a tolerable flaw-length-before-failure i.e. a maximum crack length that can be tolerated before catastrophic failure at a stress equal to the yield strength. In order to determine this critical crack length (through-thickness) the following equation was used:

$$K_{Ic} = \sigma\ (\pi a)^{0.5} \qquad (7.2)$$

with σ the flow stress in MPa (determined through tensile tests - see section 7.3)

a the critical crack length in m

The critical crack lengths were determined by using the calculated K_{Ic} values and actual, measured yield stress values. The same yield strength value was used for all the specimens of a particular heat treatment. This represents a conservative approach, as the yield stress values are higher than the operational stresses to which the chains are exposed.

The critical crack lengths are shown in figure 7.3. It is indicated by these results that in the worst scenario, the maximum flaw length that can be tolerated is 0.3 mm at a stress equal to the yield strength of 860 MPa (specimen solution treated at 930°C, cold rolled and aged at 475°C for 8 minutes). For the specimens solution treated at 880°C, aging results in a maximum allowable flaw length of 0.8 mm for 8 minutes at 475°C (for a stress of 760 MPa). See also Appendix 14 for the range of values.

It is important to emphasise that these results are for tests at room temperature; the fracture toughness is expected to drop further at lower temperatures - which would be of importance should the chains be used in a refrigeration plant.

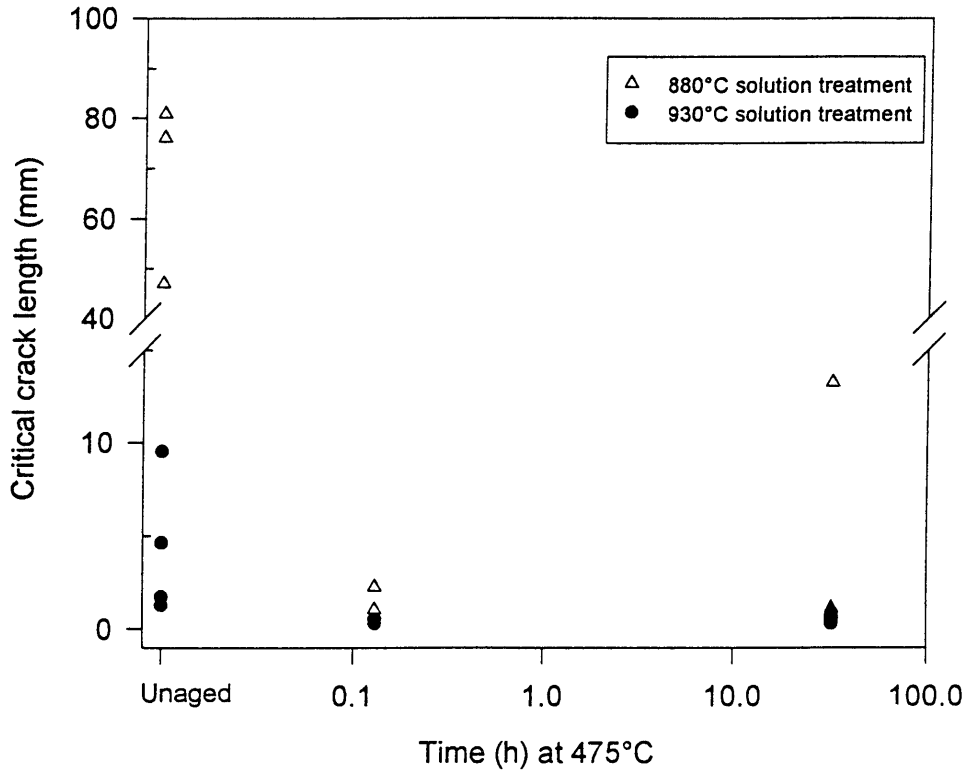

***Figure 7.3**: Calculated critical crack lengths (in mm) of specimens solution treated at 880 ℃ and 930 ℃, cold rolled and aged at 475 ℃, indicating a maximum allowable flaw length of 0.3 mm for 930 ℃ solution treatment, and 0.8 mm for 880 ℃*

The critical crack length (for the 880°C solution treatments) is comparable to the thickness of the chain links (3 mm). It is not expected that there would be flaws of this (calculated) size in the as-manufactured links. Hence, for catastrophic failure to occur, a fatigue crack must first be initiated. Therefore, fatigue is expected to determine the practical lifetime of the chains, although the lower K_{Ic} values indicate that less crack propagation will be tolerated before brittle fracture.

7.2. Fracture surfaces

The fracture surfaces were examined with the aid of a scanning electron microscope.

As expected from the low impact strength, fracture occurred mostly through brittle transgranular cleavage (figure 7.4a), accompanied by some ductile fracture (the fine equi-axed dimple structure) at the grain boundaries (figure 7.4b). In the cold worked condition grain boundaries are no longer the preferred nucleation points for cracks; rather, nucleation occurs at dislocations. This causes the matrix to be brittle, and the grain boundaries to be relatively ductile. The fine dimple structure (figure 7.5a) may well be caused by the carbide particles increasing the number of localised strain centres, initiating microvoids which grow until the ligaments between them fracture (Dieter 1988). Such a condition should also improve the capacity of the alloy to accommodate strain and limit strain concentration at the grain boundaries (Chun and Polonis 1992).

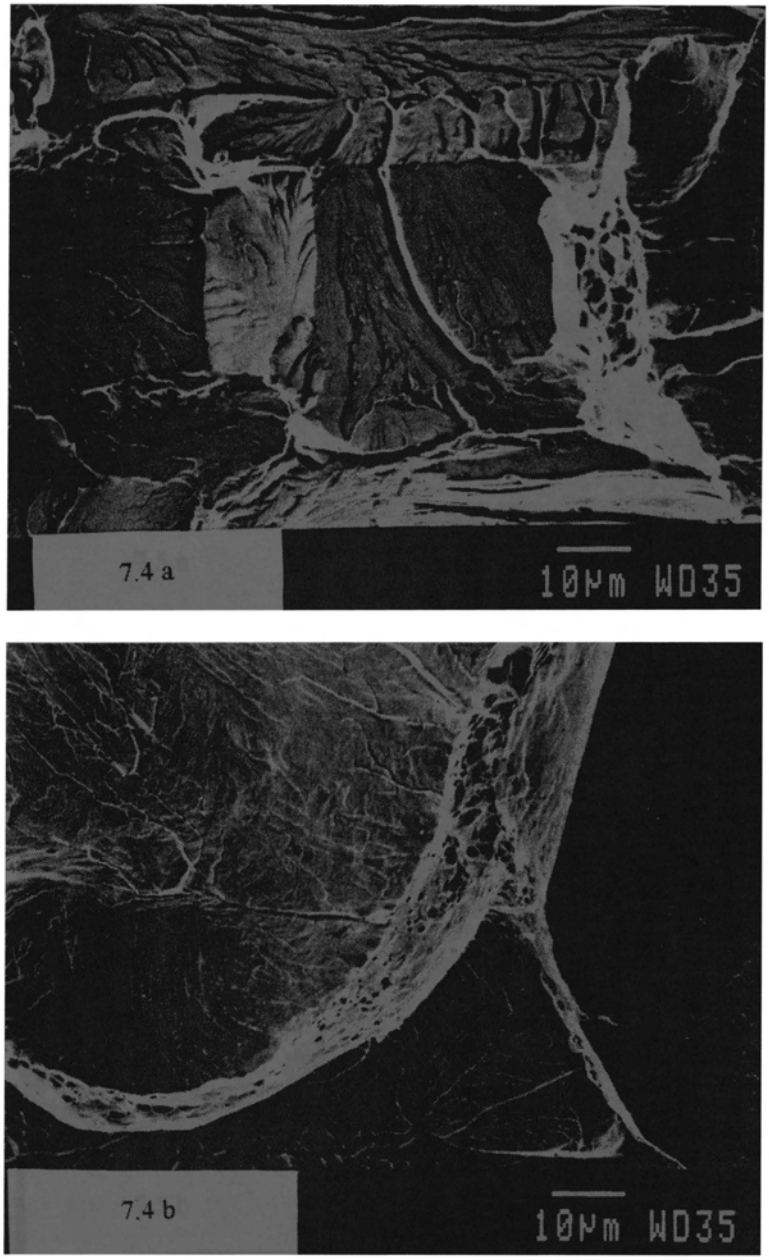

***Figure 7.4**: SEM photos of fracture surfaces (a) Transgranular cleavage fracture (930 ℃ solution treatment, aged at 475 ℃ for 277 hours (b) Ductile fracture at grain boundaries (880 ℃ solution treatment, aged at 475 ℃ for 8 minutes)*

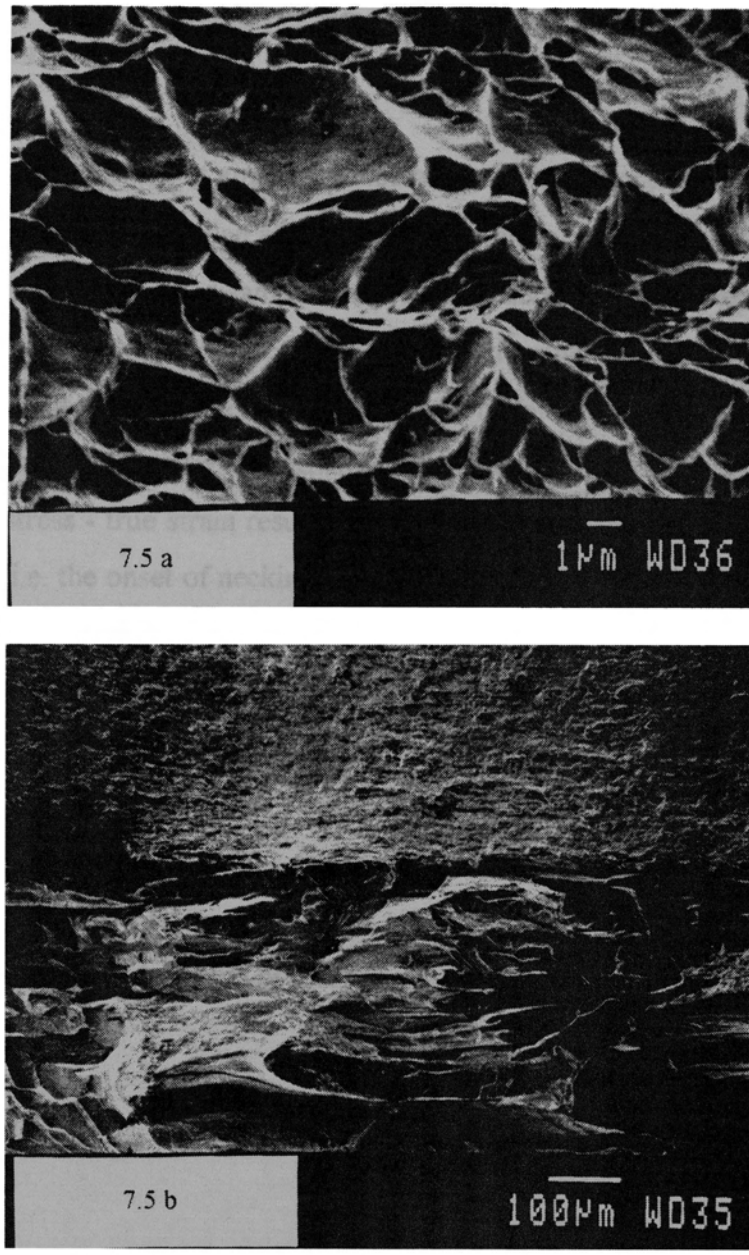

***Figure 7.5**: SEM photos of fracture surfaces (a) Microvoid coalescence (solution treatment at 880 ℃ and aged for 8 minutes at 475 ℃) (b) Transition between shear and cleavage fracture zones of an unaged specimen, solution heat treated at 880 ℃ and cold rolled; having an impact strength of approximately 150 J/cm^2*

In the samples solution treated at 880 °C microvoid coalescence was clearly visible in the regions close to the notch - figure 7.5a. The transition between shear and cleavage fracture zones was also very prominent (figure 7.5b). Crack-dividing delamination effects were prominent, which probably increased the impact strength.

7.3 Tensile tests

Tensile tests were performed at ambient temperature on specimens solution treated at 880°C and 930°C respectively, cold rolled after quenching in brine, and aged at 475°C for 8 minutes, 32 hours and 277 hours. Unaged samples, as well as undeformed and unaged specimens, were also tested. Elongation was measured using a 15 mm gauge length. This is not a standard gauge length for the specific specimen cross-section. However, the tensile behaviour was measured to compare the plastic flow characteristics. These are properly studied by comparing true stress - true strain results, which were only determined for stresses up to the tensile strength (i.e. the onset of necking). For these uniform elongations, the choice of gauge length does not affect the results. It should, however, be borne in mind that the total elongation to failure as measured in this work cannot be compared to that determined using standard gauge lengths. Force and elongation were converted to engineering stress and strain curves; which in turn were converted to true stress and true strain curves for strains up to the onset of necking. For the final graphs the elastic strain component (σ/E, with E = 210 GPa) was subtracted from the total true strain, to give plots of true stress vs. true plastic strain. Figure 7.6 illustrates the calculation process:

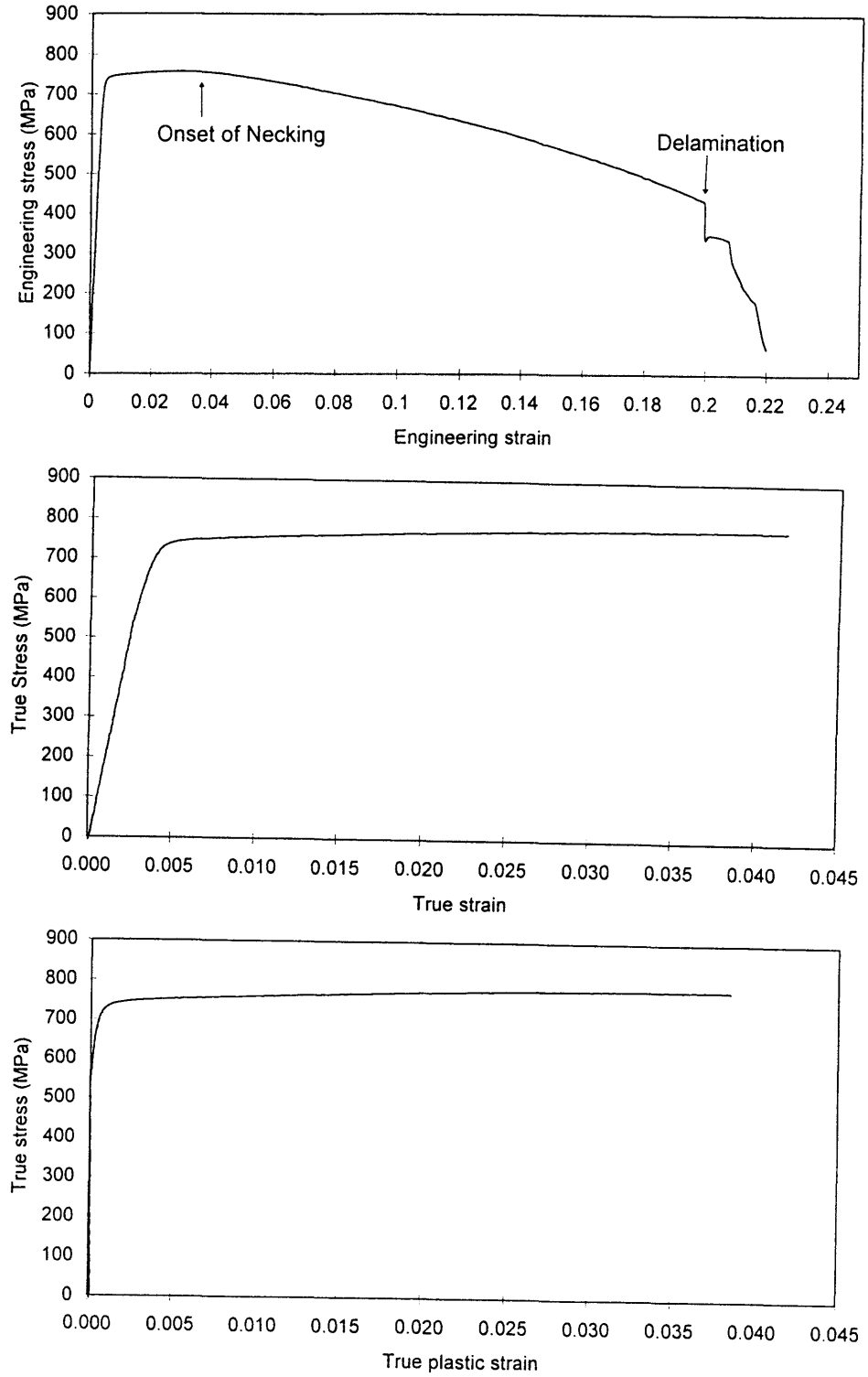

***Figure 7.6**: Results of the calculation of true stress/true plastic strain curves from engineering stress and strain values by subtracting the elastic component of the strain. The arrow in the first graph indicates the onset of delamination, which immediately preceded ductile fracture*

Some typical true stress/true plastic strain curves of the undeformed material are given in figure 7.7, and those of the cold rolled and aged specimens in figure 7.9. Figure 7.8 presents

the engineering stress/strain curves of both the 880°C and 930°C solution treated samples. The results of individual specimens of the same condition varied somewhat (see Appendix 15). This is attributed to the inhomogeneous nature of the original sheet, through factors such as segregation during solidification. It was attempted to minimise bias from just such irregularities by selecting the specimens from different positions in the sheet; and this is probably the reason for the differences in results.

The reduction in area, induced by the cold rolling, can be taken into account in the true strain values by using the following equation:

$$\text{true } \varepsilon = \ln A_0/A \qquad (7.3)$$

and in this case the 38% reduction in area amounts to a true strain of 0.478.

It can be seen from figure 7.7 that this means that the cold rolling deforms the material to well past the maximum uniform tensile elongation (i.e. the onset of necking during tensile testing).

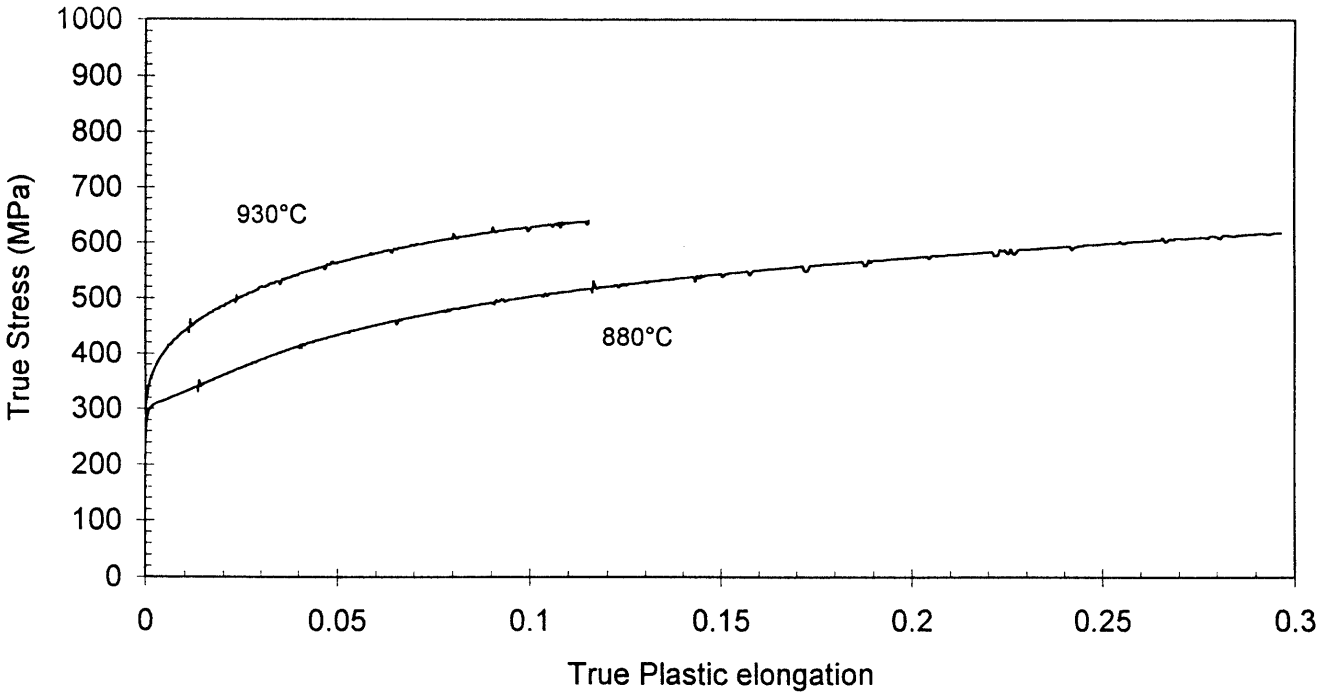

***Figure 7.7**: Typical true stress/true plastic strain curves of undeformed samples (solution heat treated at both 880℃ and 930℃, and quenched in brine). The curves terminate at the maximum uniform elongation. The values indicate that the subsequent 38% reduction in area through cold rolling (true $\varepsilon = 0.478$) is well past the available uniform tensile elongation*

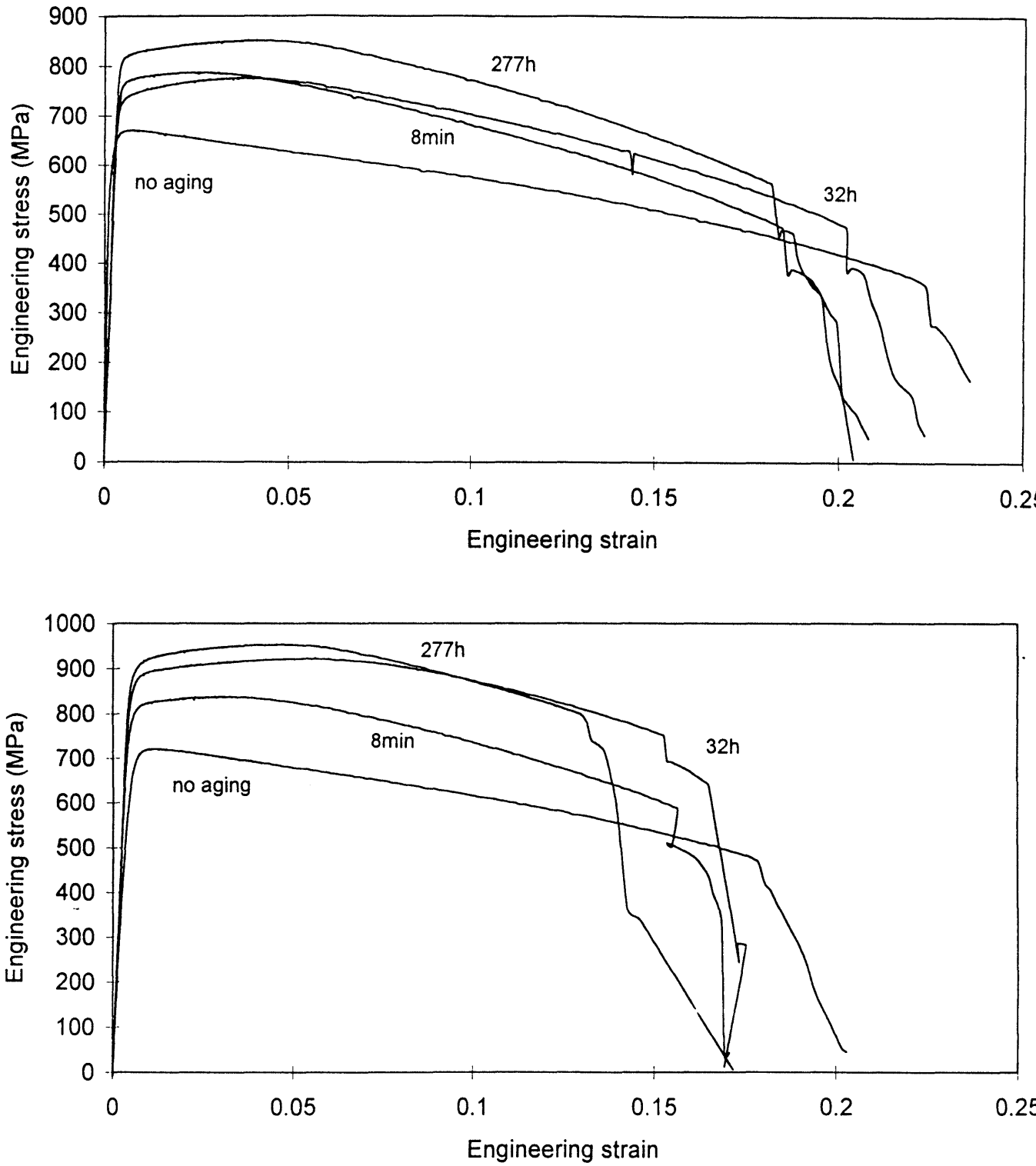

***Figure 7.8**: Typical engineering stress/strain curves of cold rolled samples (solution heat treated at (a) 880℃ and (b) 930℃, quenched in brine); and aged at 475℃ for 8 minutes, 32 hours and 277 hours. Unaged specimens are also shown*

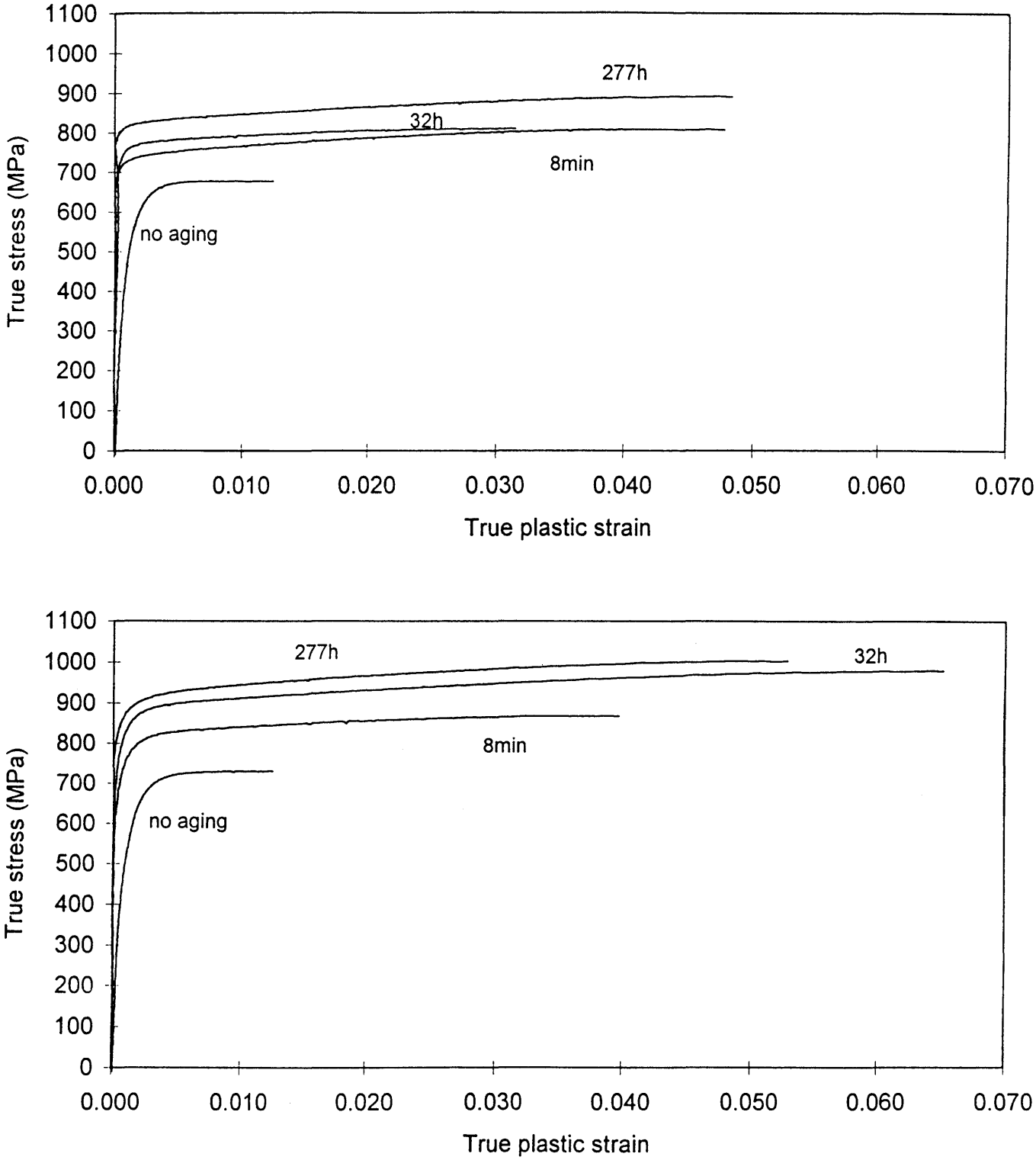

***Figure 7.9**: True stress/true plastic strain of cold rolled samples (solution heat treated at (a) 880℃ and (b) 930℃, quenched in brine); and aged at 475℃ for 8 minutes, 32 hours and 277 hours. Unaged specimens are also shown*

From figures 7.7 and 7.9 it can be seen that an increase in strength is obtained with cold rolling and aging. This increase is probably due to the increase in dislocation density (during cold rolling) and precipitation of carbides and nitrides (during aging); both effects impede dislocation motion. Without aging, little uniform elongation occurs before the onset of necking, in line with the observation that the deformation during cold rolling is larger than the uniform tensile elongation of the undeformed material. The maximum uniform plastic deformation increases in the first aging step (figure 7.10), but is similar for subsequent aging. This is linked to the work hardening rate, which will be discussed later in this section.

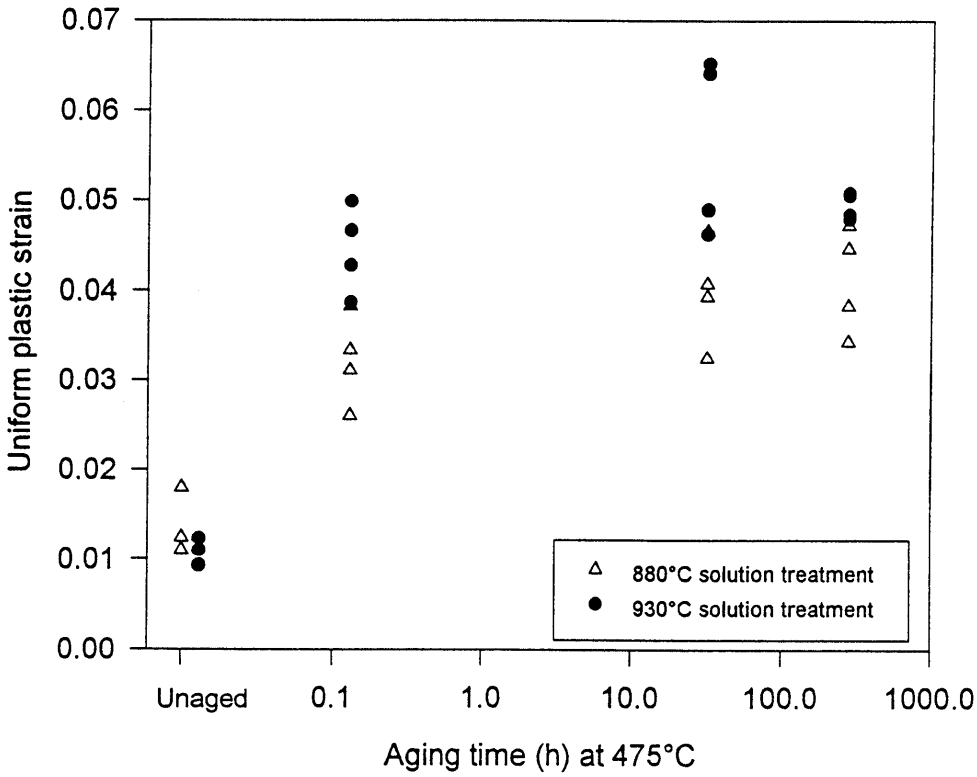

***Figure 7.10**: Uniform plastic strain (true strain at the onset of necking). Results indicate that the uniform plastic strain increases in the first aging step*

Two further aspects arise from the results shown in figures 7.8 and 7.9. The first is that, in the unaged material, plastic flow occurs immediately upon application of an external stress - no elastic region is observed. This is attributed to the residual stresses which arise as a result of cold rolling. During cold rolling deformation is not homogeneous through the thickness of the material. The centre of the material tends to restrain the surface from elongation. The result is a residual stress pattern which consists of a high compressive stress at the surface and a tensile stress at the centre. Because of the residual stresses, parts of the material are at, or

close to, the tensile yield stress, even with no externally applied stress. This causes the material to exhibit macroscopic plastic flow even at low applied stress, as is evident in the tensile behaviour of the as-rolled material (figures 7.8 and 7.9).

Metals containing residual stresses can be stress relieved, by heating to a temperature where the yield stress of the material is the same or less than the value of the residual stresses, thus allowing the material to deform and release the stress (Dieter 1988, p. 557). With aging, even after only 8 minutes at 475°C, these residual stresses are relieved, as is evident from the tensile results. This behaviour was noticed in both the 880°C and 930°C solution treated specimens and is in accordance with the results seen in the TEM micrographs, showing recovery (section 4.3).

The second aspect arising from the curves in figures 7.8 and 7.9, is that, in addition to the relief of residual stresses, the work hardening behaviour is changed by the first aging step. This is evident from the increase in uniform elongation (figure 7.10) and in plots of the work hardening rate (θ). The work hardening rate is defined as the slope of the true stress - true strain curve ($\theta = d\bar{\sigma}/d\bar{\varepsilon}$); the results are shown in figures 7.11 and 7.12.

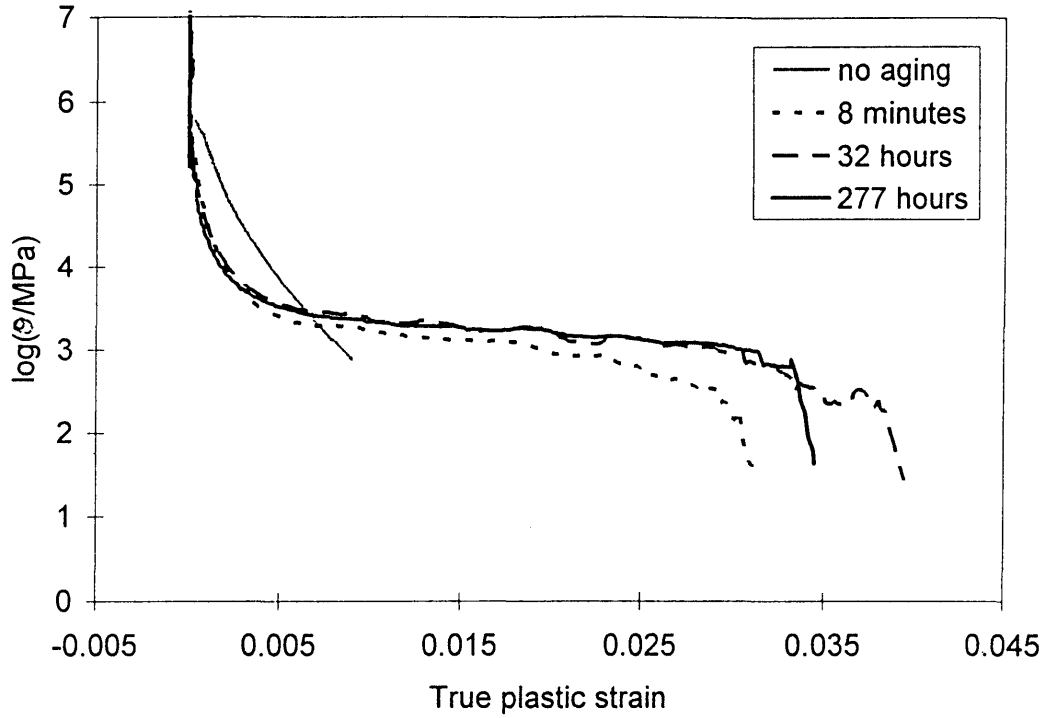

***Figure 7.11**: The effect of plastic strain on the work hardening rate (θ) of samples solution treated at 880℃, cold rolled and aged at 475℃. The results indicate a change in work hardening behaviour after the first aging step, with higher work hardening rates at higher strains for the aged specimens*

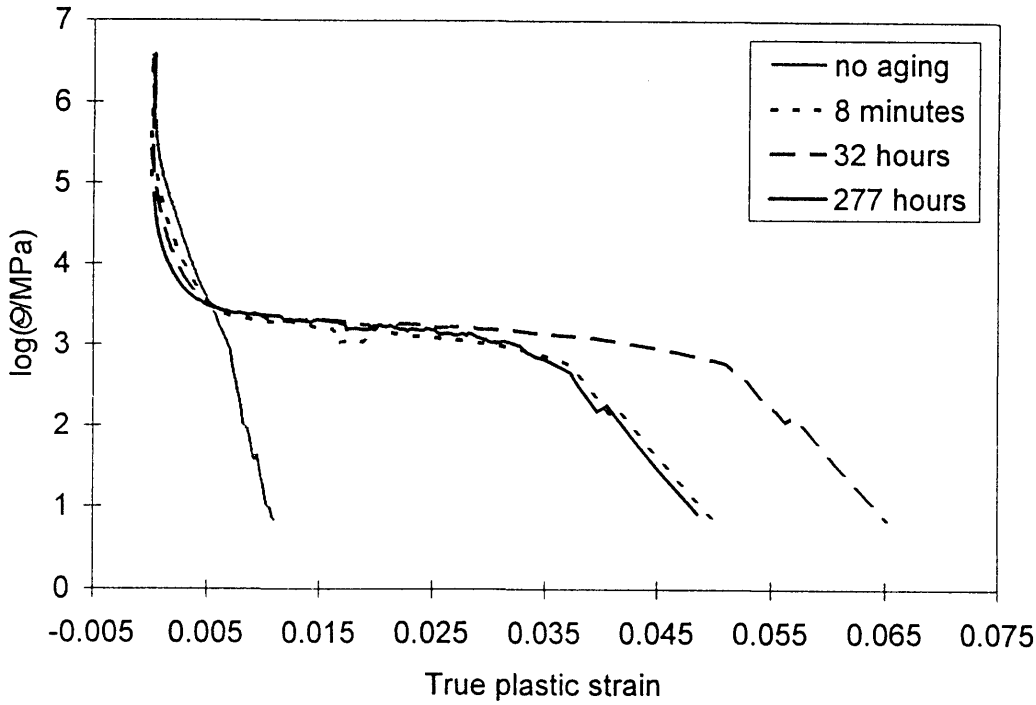

***Figure 7.12**: The effect of plastic strain on the work hardening rate (θ) of samples solution treated at 930℃, cold rolled and aged at 475℃. The results indicate a change in work hardening behaviour after the first aging step, with higher work hardening rates at higher strains for the aged specimens*

In these figures, the apparently higher initial work hardening rate of the unaged specimens results from the occurrence of flow at low applied stress (i.e. the effect of residual stresses), as is evident from figures 7.8 and 7.9. However, the work hardening rate of the unaged specimens drops below that of the aged samples at a true strain of around 0.006, resulting in the lower uniform elongation of the unaged specimens (figures 7.8, 7.9 and 7.10). The work hardening rate of all the aged specimens is similar. The higher work hardening rate of the aged specimens indicates a more rapid increase in dislocation density during deformation; this is presumably the result of the precipitation of nondeforming particles during aging.

While not of importance for the practical use of the chains, interesting effects of cold working and aging on the strain-to-fracture were found. Because of significant plastic anisotropy, the strain-to-failure is not quoted as the reduction in area; but rather as the individual strains in the width and thickness directions (figures 7.13 and 7.14). It is clear that the true strain at ductile fracture is similar for undeformed, deformed and aged material (for each prior solution treatment), with a small decrease in fracture strain after the first aging step. Figure 7.15 gives the ratio of these two strains ($\varepsilon_w/\varepsilon_t$; the R-ratio). Statistically there is little difference between the true strains-to-ductile fracture in the width direction, in the true strain-to-ductile fracture in the thickness direction of the aged specimens, or between the deformed and undeformed samples (no aging involved in either case). There does, however, seem to be small but significant differences between the aged and unaged specimens.

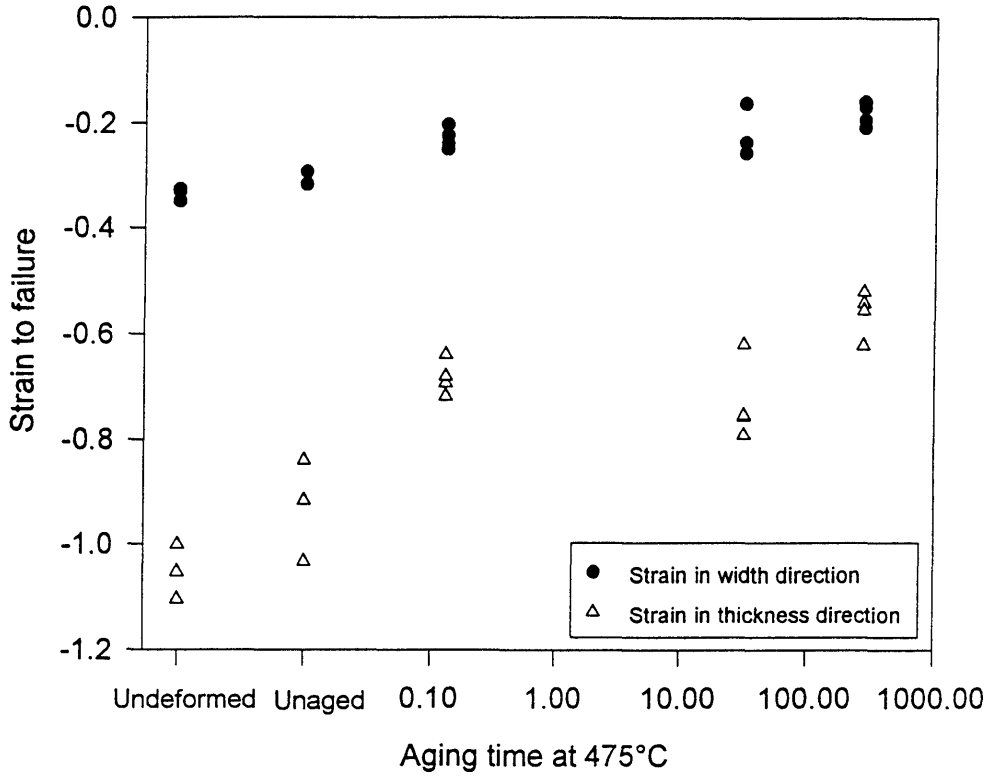

***Figure 7.13**: Strain-to-failure in the width and thickness directions of the specimens solution treated at 880℃. Results indicate that there is little difference in the true strains to ductile fracture*

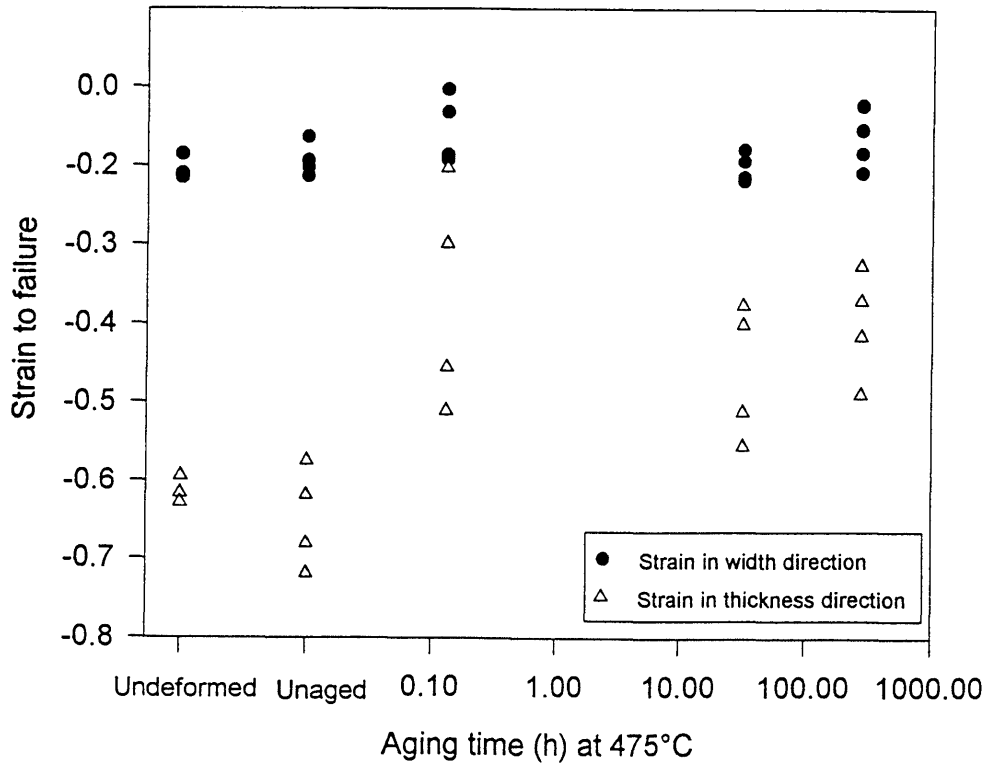

***Figure 7.14**: Strain-to-failure in the width and thickness directions of the specimens solution treated at 930℃. Results indicate that there is little difference in the true strains to ductile fracture*

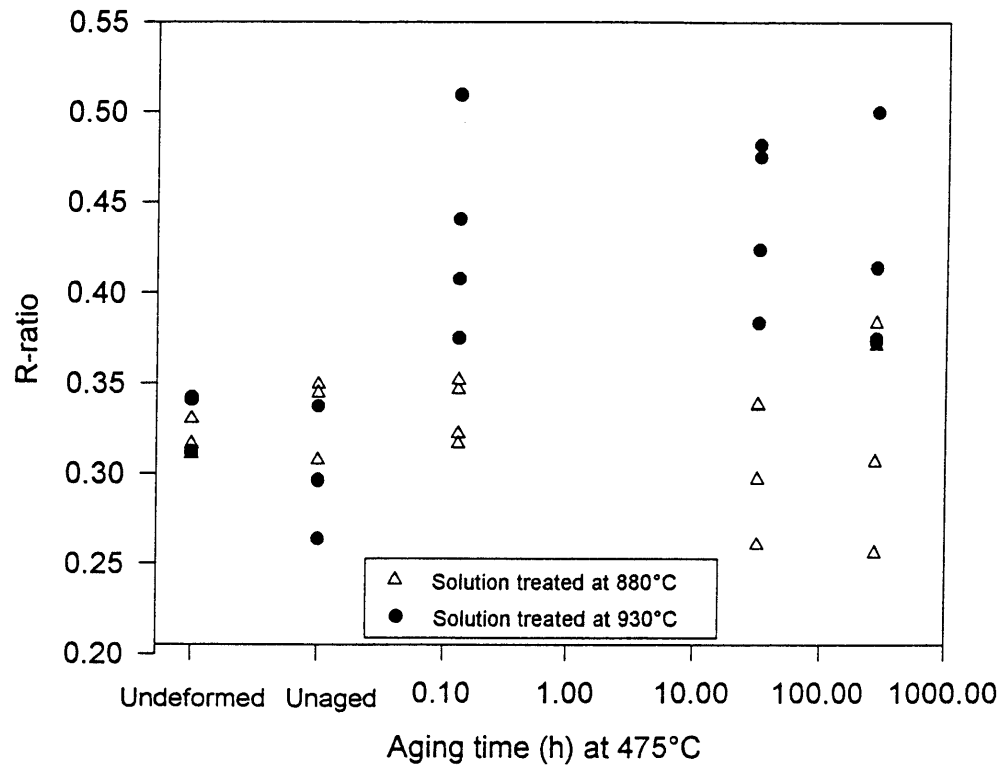

***Figure 7.15**: R-ratio of the true strains ($\bar{\varepsilon}_w/\bar{\varepsilon}_l$). Values do not differ significantly*

The similarity of the strains appear surprising at first, since the cold-rolled material had received a true strain (in the thickness direction) of $\bar{\varepsilon}_t = -0.478$, and hence a smaller true strain to ductile failure might be expected, compared to the undeformed material. However, no such large reduction in fracture strain is observed. Based on the roughly constant R-ratio (figure 7.15), it is also not expected that the crystallographic texture is much changed by the cold rolling.

This effect is explicable with reference to the way in which the final ductile fracture occurs. Figure 7.6 shows that fracture was preceded by an irregular decrease in load. This irregular decrease was not an artefact of the tensile testing machine, but was observed to coincide with delamination (parallel to the rolling direction and in the rolling plane). Delamination occurs as a result of the triaxial stresses which develop in the neck (Dieter 1988, p.292). The magnitude of the triaxial stress depends on the average (applied) stress, and the ratio of the radius of curvature of the neck to specimen linear cross section. This latter ratio correlates with $\Delta\varepsilon_t$ (the difference between the true strain at fracture and the true strain at necking) (ibid.). Figure

7.16 shows this difference for the various heat treatment conditions. $\bar{\varepsilon}_{t,n}$ (true strain at necking) was determined as follows:

$$\bar{\varepsilon}_l + \bar{\varepsilon}_w + \bar{\varepsilon}_t = 0 \qquad \text{(constancy of volume)} \qquad (7.5)$$

with $\bar{\varepsilon}_l$ the true strain in the length direction

$\bar{\varepsilon}_w$ the true strain in the width direction

$\bar{\varepsilon}_t$ the true strain in the thickness direction

and

$$\bar{\varepsilon}_{w,n} = R\bar{\varepsilon}_{t,n} \qquad (7.6)$$

with $\bar{\varepsilon}_{w,n}$ the true strain in the width direction, at necking

$\bar{\varepsilon}_{t,n}$ the true strain in the thickness direction, at necking

$R = \bar{\varepsilon}_{w,f}/\bar{\varepsilon}_{t,f}$ (at fracture), and presumably applicable at the onset of necking too

thus

$$\bar{\varepsilon}_{l,n} + (1+R)\bar{\varepsilon}_{t,n} = 0$$

$$\bar{\varepsilon}_{t,n} = -\bar{\varepsilon}_{l,n}/(1+R) \qquad (7.7)$$

with $\bar{\varepsilon}_{l,n}$ the uniform elongation up to the onset of necking

$\Delta\bar{\varepsilon}_t$ (difference between true strain at fracture and true strain at necking) was determined by subtracting $\bar{\varepsilon}_{t,n}$ from $\bar{\varepsilon}_{t,f}$ (true strain at fracture in the thickness direction).

The figure demonstrates that the neck morphology at fracture is similar for all the specimens. Figure 7.17 gives the traced outlines of the tensile specimens after fracture. It indicates that correlation between the form of the neck and the uniformly elongated region next to the neck is similar for all the tested specimens, the deformed, undeformed and aged.

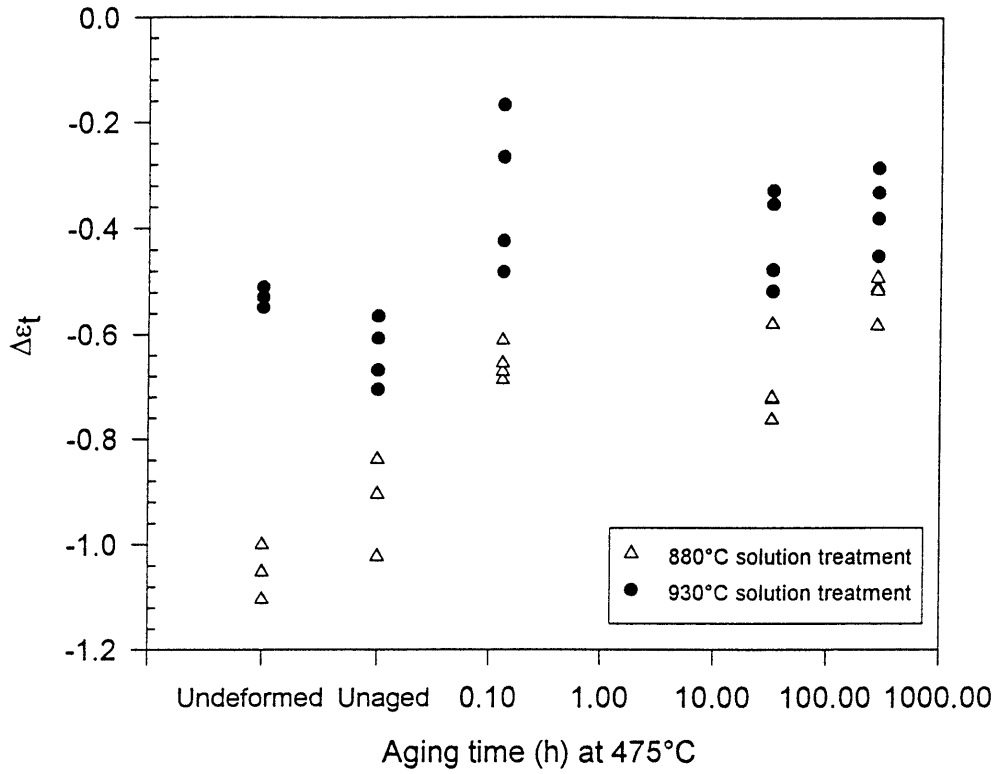

***Figure 7.16**: Difference between the true strain in the neck at fracture and true strain at necking (in the thickness direction) giving an indication of the shape of the neck of the tensile specimen at fracture. Results indicate that the shape of the neck - giving rise to triaxial stress - is similar for all the specimens*

***Figure 7.17a**: Outlines of the necks after fracture of the deformed and undeformed specimens (specimens solution treated at 880 ℃). The neck shapes are similar for all the specimens and delamination cracks can be seen*

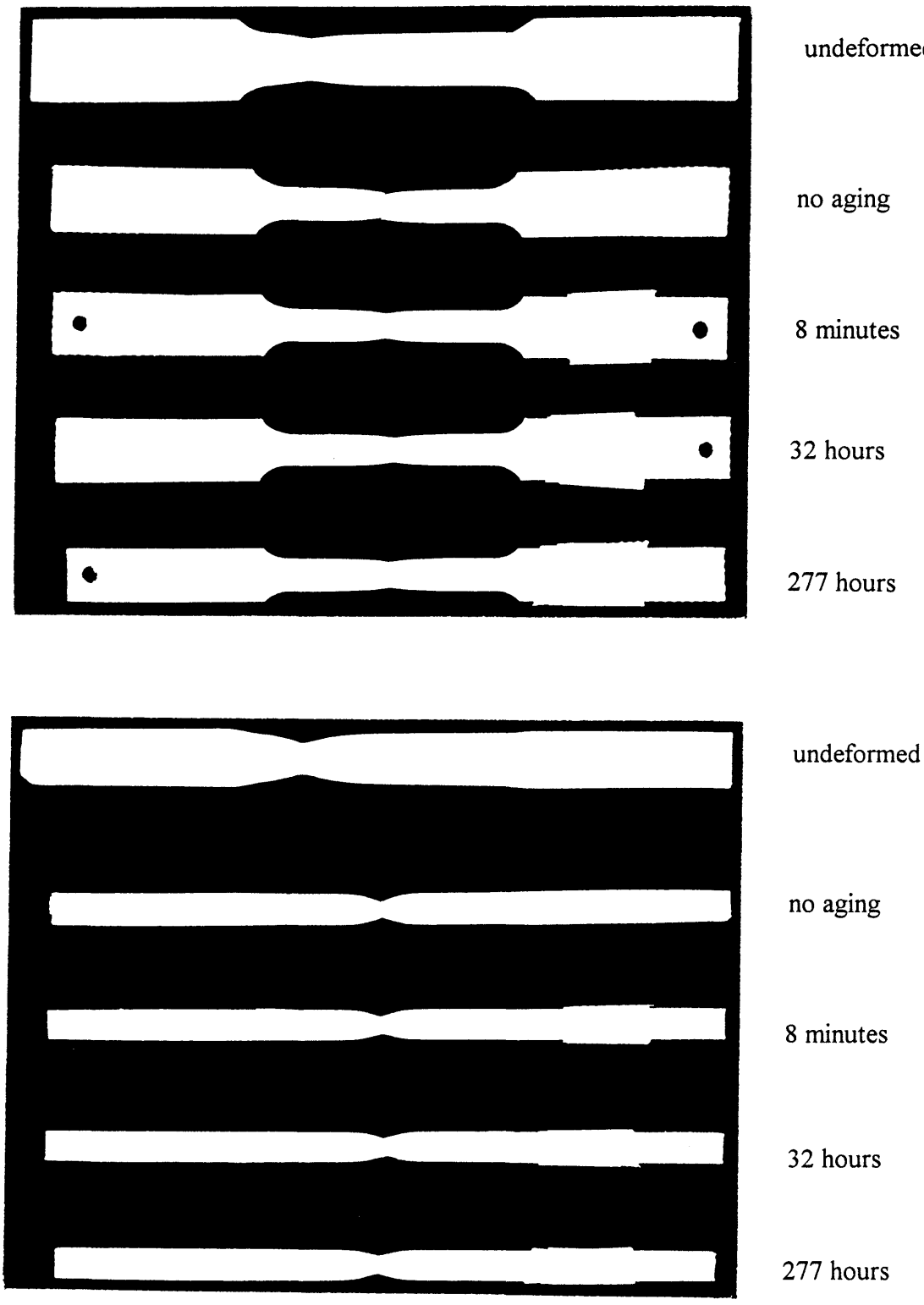

***Figure 7.17b**: Outlines of the necks after fracture of the deformed and undeformed specimens (specimens solution treated at 930 ℃). The neck shapes are similar for all the specimens and delamination cracks can be seen*

In the light of the similar flow stress (figures 7.7 to 7.9) and neck morphology, it is deduced that the triaxial stress assumes a similar value at fracture in all the specimens, in line with the observed role of delamination immediately before ductile fracture.

7.4 Summary of mechanical properties

The mechanical properties (hardness - figure 7.18, tensile strength and yield stress - figure 7.19) exhibit similar trends, namely significant increases in the first aging step (8 minutes), and again at long periods of aging (more than 64 hours). Toughness, however, is sacrificed with the increased strength (figure 7.20), and shows the expected decrease, as embrittlement proceeds. Figure 7.20 was constructed by measuring the hardness of the impact specimens, and converting it into yield strength, with the relationship:

yield strength = 6.291×hardness - 920.07 (7.8)

with yield strength in MPa and Vickers hardness in kg/mm^2

This relationship was obtained by plotting the measured yield strengths (section 7.3) as a function of the hardness of the impact specimens.

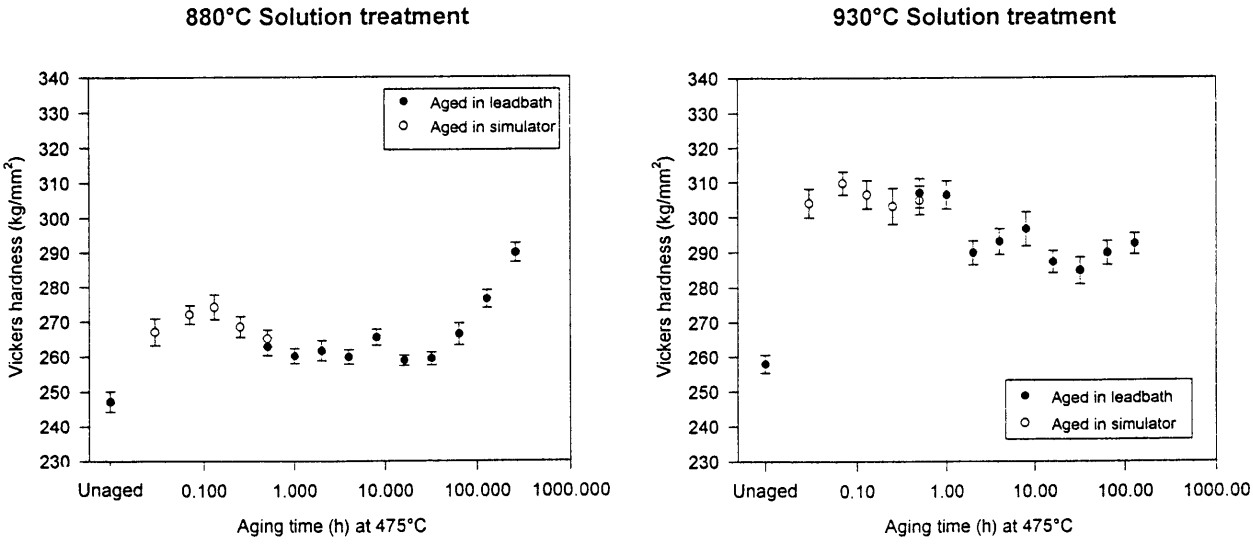

Figure 7.18: Hardness curves of samples solution treated at 880 ℃ and 930 ℃, cold rolled and aged at 475 ℃

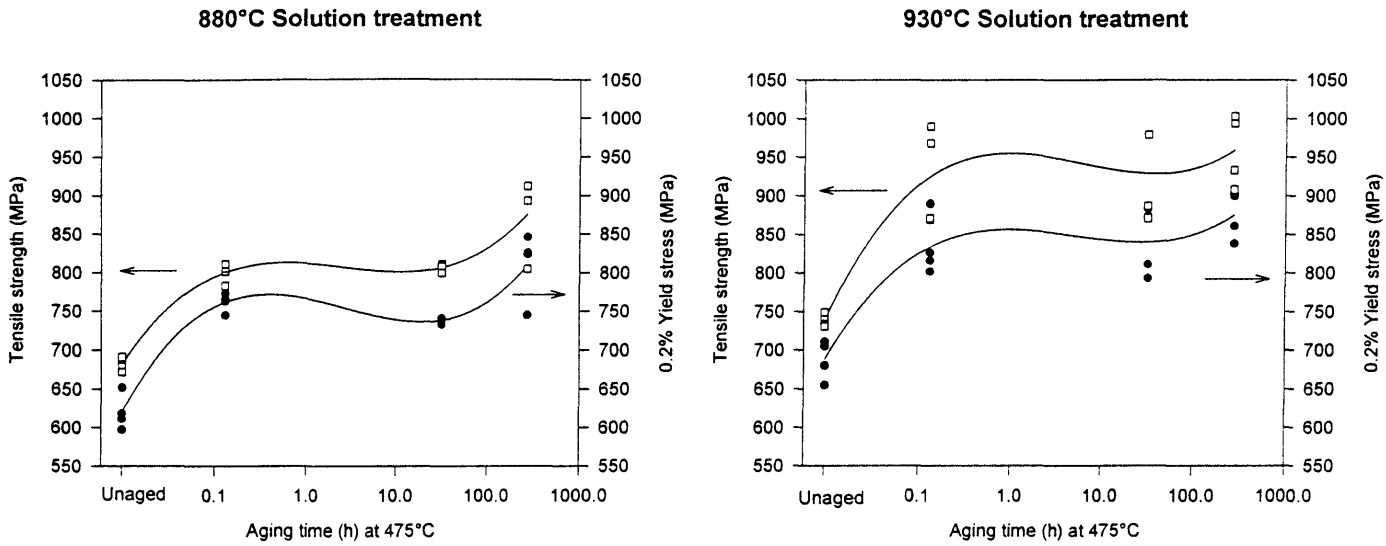

***Figure 7.19**: Tensile strength and 0.2% yield stress of samples solution treated at 880 ℃ and 930 ℃, cold rolled and aged at 475 ℃*

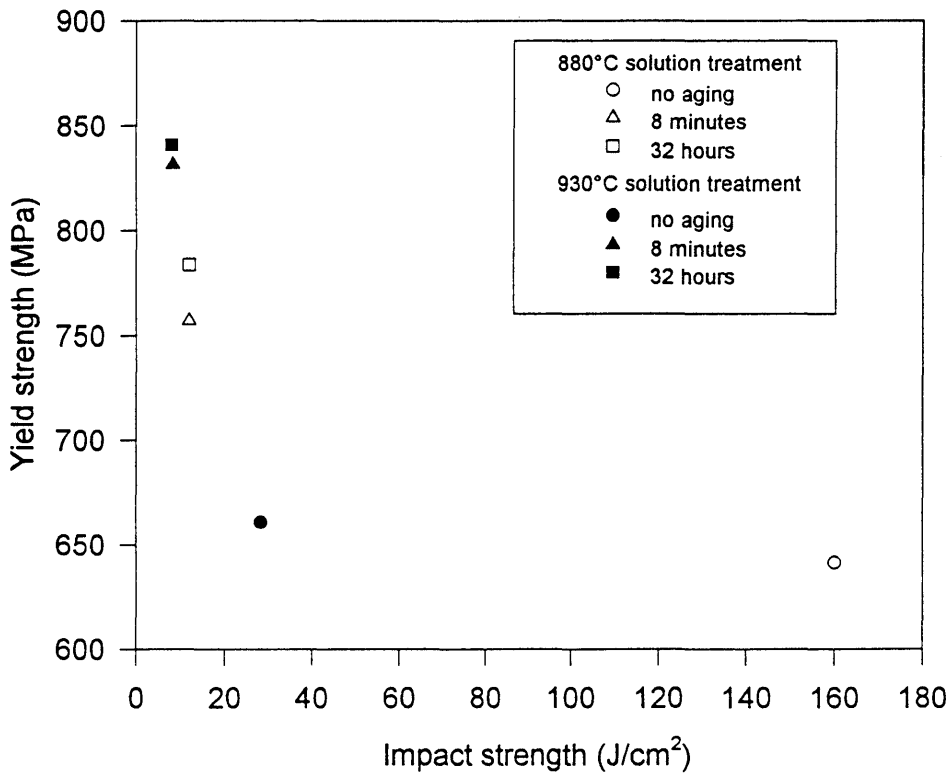

***Figure 7.20**: A plot of the average strength and toughness values which indicated that there is not a significant difference between the relationship, for both the 880 ℃ and 930 ℃ solution treatments*

7.5 Conclusions

Toughness is severely reduced by the aging treatments; fracture occurs mostly through transgranular cleavage fracture.

At worst, a maximum critical crack length of 0.3 mm can be tolerated before catastrophic failure, at a stress corresponding to the yield strength of 860 MPa, for specimens solution treated at 930°C and aged for 8 minutes at 475°C. For solution treatment at 880°C, a maximum crack length of 0.8 mm can be tolerated, but at a lower stress. Fatigue is expected to determine the lifetime of the chains, although the low K_{Ic} values indicate that less crack propagation will be tolerated before brittle fracture.

After the first aging step (8 minutes of aging), increases in the work hardening rate and uniform elongation are observed, and the residual stresses from cold rolling are apparently largely removed. Little change in work hardening behaviour occurs with subsequent aging.
The true strain at ductile fracture is similar in all cases, in line with the observation that delamination occurs (as a result of triaxial stresses in the neck) immediately before ductile fracture.

Tensile strength and 0.2% yield strength exhibit the same behaviour as the hardness, namely an initial increase at short aging times and a second increase at longer periods of aging, in support of the contention that two strengthening mechanisms are involved: the precipitation of carbides and nitrides at short aging periods, and the formation of α" at long periods of aging.

Chapter 8

Effect of Cold Rolling and Heat Treatments on Corrosion Resistance

Due to the surroundings in which the slat band chains are used, general corrosion resistance is a necessity. It is therefore of importance to determine the effect of the strengthening treatments on corrosion properties. To measure the resistance to general corrosion the material was potentiodynamically tested in a 0.5M H_2SO_4 solution, since reducing acids such as sulphuric acid commonly cause general corrosion of stainless steels. A change in polarisation behaviour of the steel in this solution would indicate a change in the general corrosion resistance, even though this solution is more aggressive than the actual environment to which the chains are exposed during use.

8.1. No solution treatment, solution treatment at 880°C and 930°C

No signs of a decrease in general corrosion resistance could be observed after any of the treatments. That is to say, with and without solution treatments, with cold rolling and with aging for up to three months - figure 8.1. This is consistent with results obtained by other authors (Aggen *et al.* 1978, Cortie 1995)

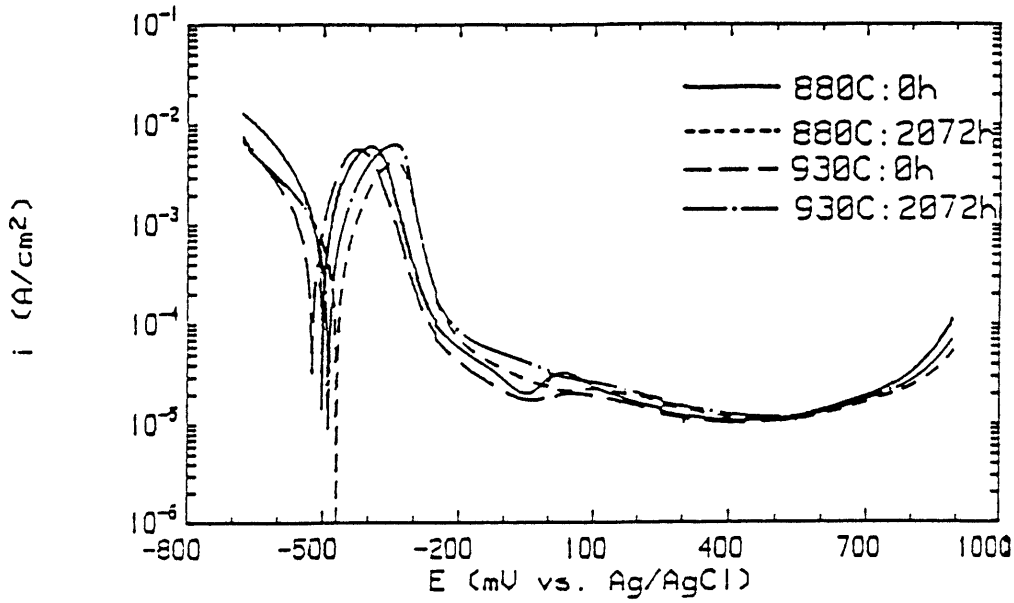

***Figure 8.1**: Polarisation diagrams of (a) solution treatment at 880 ℃, no aging; (b) solution treatment at 880 ℃, aging at 475 ℃ for 2072 hours; (c) solution treatment at 930 ℃, no aging and (d) solution treatment at 930 ℃, aging at 475 ℃ for 2072 hours, indicating that aging has little on no effect on the polarisation behaviour*

Investigation of the pitting corrosion resistance (3.56% NaCl solution) revealed that this property is not affected either, at least not without additional solution treatments before aging at 475°C (figure 8.2).

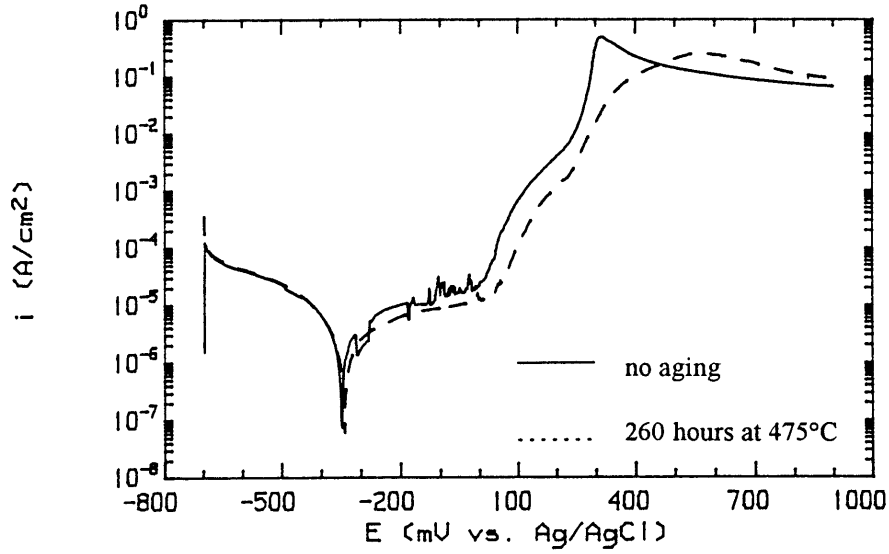

***Figure 8.2**: Pitting corrosion tests of specimens (a) with and (b) without aging (260 hours at 475 ℃) after cold rolling. No additional solution heat teatments. Tested in 3.56% NaCl. Aging does not affect the pitting potential, which is approximately 0.0 $V_{Ag/AgCl}$ in both cases*

The general corrosion properties of the chain links were not affected by any treatments (aging at 100°C, 450°C and 475°C) either.

8.2. Solution treatment at 990°C

With aging at 475°C, after solution treatment at 990°C and cold rolling, pronounced second anodic current peaks appeared after just 2 hours of aging. These peaks disappeared again after about 64 hours at temperature.

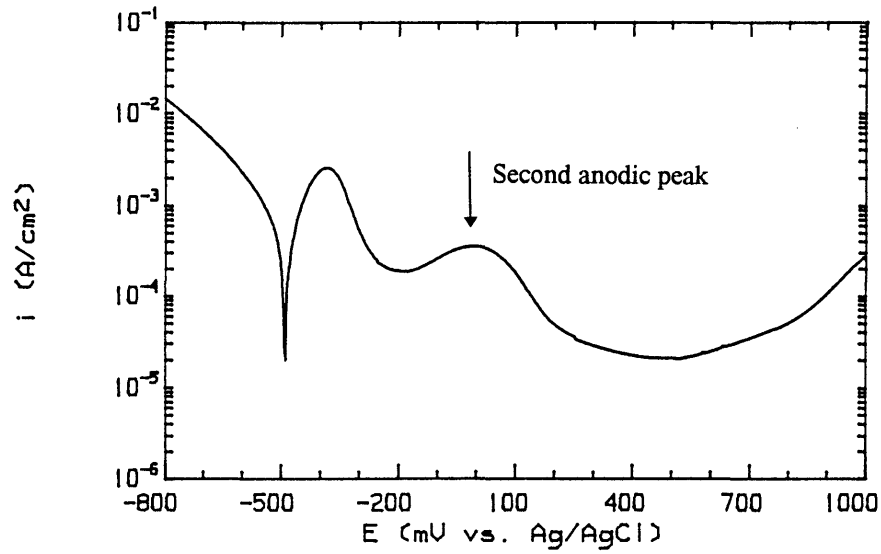

***Figure 8.3**:Second anodic current peak in sample aged at 475℃ for 16 hours (solution treatment at 990℃)*

The fact that corrosion does occur (when these peaks are visible) was confirmed by potentiostatic testing - 5 minutes at 0V - in the 0.5M H_2SO_4 solution. At this potential regions containing less than 12% Cr are active, while more Cr-rich areas are passive (Kirchheim *et al.* 1989). Thus if the measured current density is relatively high, the presence of chromium-depleted regions is inferred. At 0V the second annodic current peaks reached a maximum. The increase of the current density from 1×10^{-4} A/cm^2 to 7×10^{-3} A/cm^2 (figure 8.4) is indicative of active corrosion.

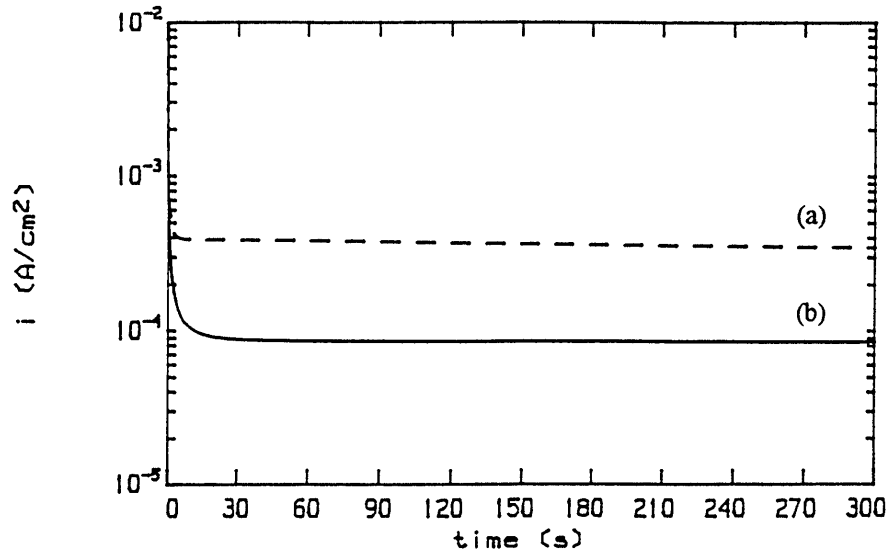

***Figure 8.4**: Potentiostatic tests at 0 V in 0.5M H_2SO_4 of samples (a) aged at 475 ℃ for 16 hours and (b) before aging (solution treatment at 990 ℃). The higher current density in (a) indicates that active corrosion occurs*

The reason for the observed current peak is thought to be sensitisation (Cr depletion of the matrix) associated with precipitation of Cr-rich carbides and nitrides. The disappearence after long periods of aging is probably due to recovery as sufficient chromium diffusion takes place to replenish the impoverised regions.

8.3. Cold work

Cold work does not influence the corrosion resistance as aging proceeds. No change was observed in the polarisation behaviour after cold rolling. These results are discussed in section 4.1.2.

8.4. Solution treatments without cold working

Only after solution treatments at temperatures higher than 1075°C were any signs of deterioration in corrosion properties observed. Second anodic current peaks became evident after solution treatment at these temperatures.

8.5. Conclusions

The heat treatments can be applied to the commercial product, as they do not affect the general corrosion resistance of the material. This is probably because the chromium depletion is not intergranular in nature and hence does not form continuous active regions, and the α" precipitation and its subsequent chromium depletion occur on a short length scale.

Chapter 9

Summary

The previous chapters presented results from the investigation into the possible mechanisms which cause strengthening when a 430 ferritic stainless steel is cold worked and aged in the "475°C-Embrittlement" range.

It was established that cold rolling, by increasing the dislocation density, increases the unaged hardness substantially. It also affects the short-time aging behaviour by enhancing the precipitation of carbides and nitrides. It was found that strain aging does not significantly influence the strength, and that recovery takes place with aging.

It was determined that the short-time aging behaviour is largely governed by the precipitation of carbides and nitrides. The precipitation becomes significant only when the interstitial content is increased by additional solution heat treatments before cold rolling and aging. It was established through Mössbauer studies that the precipitates are most likely chromium-rich. The increased work hardening rate (observed during tensile testing) also testifies to the precipitation of nondeforming particles during aging.

The additional solution heat treatments, if performed above the Ac_1 temperature, introduce martensite into the matrix, which increases the unaged hardness, seemingly without affecting the corrosion resistance.

Only after long periods of aging (more than 64 hours) does the Cr-precipitate (α") - usually associated with "475°C-embrittlement" - influence the hardness.

These treatments do not affect the corrosion resistance and passivation behaviour.

Both impact strength and lateral expansion indicate that embrittlement accompanies the increased strength obtained by aging. Calculated critical crack lengths from the impact data,

however, revealed that the maximum flaw length of 0.8 mm (for specimens solution treated at 880°C) is comparable to the thickness of the chains (3 mm). Since it is not expected that flaws of that size will exist in the as-manufactured links, fatigue will probably determine the lifetime of the chains, although the lower K_{Ic} values indicate that less crack propagation will be tolerated before brittle fracture.

In conclusion it can be said that the cold working and heat treatments seem to be an easy and cost-effective method for increased strength, which would prolong conveyor life.